



Geochemistry, Geophysics, Geosystems

RESEARCH ARTICLE

10.1029/2019GC008843

Key Points:

- Moderately reduced shear wave velocities ($\Delta V_s \sim 4\text{--}10\%$) relative to surrounding lithosphere are observed in the upper mantle beneath the Malawi Rift and the Rungwe Volcanic Province
- Localized low velocities beneath Rungwe can be explained by modestly elevated temperatures and preclude significant melt
- Shear wave velocity structure beneath the Malawi Rift suggests lithospheric modification localized along ancient sutures enabled initiation of rifting

Supporting Information:

- Supporting Information S1

Correspondence to:

J. B. Gaherty,
james.gaherty@nau.edu

Citation:

Accardo, N. J., Gaherty, J. B., Shillington, D. J., Hopper, E., Nyblade, A. A., Ebinger, C. J., et al. (2020). Thermochemical modification of the upper mantle beneath the northern Malawi Rift constrained from shear velocity imaging. *Geochemistry, Geophysics, Geosystems*, 21, e2019GC008843. <https://doi.org/10.1029/2019GC008843>

Received 21 NOV 2019

Accepted 22 APR 2020

Accepted article online 25 APR 2020

Thermochemical Modification of the Upper Mantle Beneath the Northern Malawi Rift Constrained From Shear Velocity Imaging

N. J. Accardo¹ , J. B. Gaherty^{2,3} , D. J. Shillington^{2,3} , E. Hopper² , A. A. Nyblade¹ , C. J. Ebinger⁴ , C. A. Scholz⁵ , P. R. N. Chindandali⁶ , R. Wambura-Ferdinand⁷, G. Mbogoni⁸, J. B. Russell² , B. K. Holtzman² , C. Havlin² , and C. Class²

¹Department of Geosciences, Pennsylvania State University, State College, PA, USA, ²Lamont-Doherty Earth Observatory of Columbia University, Palisades, NY, USA, ³Now at School of Earth and Sustainability, Northern Arizona University, Flagstaff, AZ, USA, ⁴Department of Earth and Environmental Sciences, Tulane University of Louisiana, New Orleans, LA, USA, ⁵Department of Earth Sciences, Syracuse University, Syracuse, NY, USA, ⁶Malawi Geological Survey Department, Zomba, Malawi, ⁷Department of Geology, University of Dar es Salaam, Dar es Salaam, Tanzania, ⁸Geological Survey of Tanzania, Dodoma, Tanzania

Abstract To investigate the controls on continental rifting in the western branch of the East Africa Rift System, we conduct shear velocity imaging of the crust and uppermost mantle beneath the weakly extended Malawi Rift and the Rungwe Volcanic Province (RVP). We use local-scale measurements of Rayleigh wave phase velocities between 9- and 100-s periods combined with constraints on basin architecture and crustal thickness to invert for shear velocity from the surface to ~135 km. Our resulting 3-D model reveals a localized low-velocity anomaly associated with the RVP extending from the crust and through the upper mantle, which can be explained with modestly elevated temperatures. Away from the RVP, velocities within mantle flanking the rift are fast ($>4.6 \pm 0.1$ km/s), suggesting depleted lithospheric mantle to depths of ~100 and >135 km to the west and east of the rift, respectively. The upper mantle beneath the rift axis is characterized by thinned lithosphere with slower velocities than the surrounding plateau, suggestive of thermal and/or chemical modification by the rifting process. Slowest velocities are mildly asymmetric about the rift axis, with the lowest velocities observed beneath the rift and adjacent footwall escarpments. The underlying asthenosphere is only moderately slow ($\sim 4.25 \pm 0.1$ km/s), including beneath the RVP, precluding the presence of significant volumes of partial melt. The positions of localized lithospheric modification and basin-bounding border faults correlate with the location of Proterozoic mobile belts, suggesting that these sutures provide lithospheric-scale weakening mechanisms necessary for localizing strain and allowing extension to occur in the Malawi Rift.

1. Introduction

Debate surrounds the mechanisms enabling continental extension in strong, cold, and thick lithosphere beneath large sectors of the East African Rift System (EARS; e.g., Ebinger, 2005; Priestley & McKenzie, 2006). Given the lithospheric strength implied by these characteristics and the modest magnitude of available tectonic, gravitational, and mantle-dynamic forces (e.g., Bott, 1991; Stamps et al., 2014), weakening mechanisms are required to enable rift initiation (e.g., Buck, 2006; Regenauer-Lieb et al., 2008). Diverse geophysical studies of magma-rich rift systems have established the influential role of melt products in enabling continental rifting (e.g., Buck, 2006; Corti et al., 2003; Ebinger et al., 2017; Muirhead et al., 2016; Thybo & Nielsen, 2009; Wright et al., 2006). However, comparable understanding of the weakening mechanisms in magma-poor rift systems has yet to be found. The geologic record contains numerous examples of relatively amagmatic rifts (e.g., Newfoundland-Iberia rift; Whitmarsh et al., 2001; Van Avendonk et al., 2006), and several active rifts display evidence of (at best) very limited magmatic activity (e.g., Gulf of Corinth; Nixon et al., 2016). Modeling and geochemical studies have proposed a variety of mechanisms for inducing weakening and localized extension, including shear heating and dynamic grain size reduction (Regenauer-Lieb et al., 2008), edge-driven instabilities (e.g., King & Anderson, 1995; Koptev et al., 2018), the presence of pre-existing weaknesses like tectonic sutures (e.g., Corti et al., 2011), and widespread metasomatism of mantle lithosphere above mantle plumes (e.g., Foley & Fischer, 2017; Furman et al., 2016; Furman & Graham, 1999). Few detailed observational studies exist to test these models.

The western branch of the EARS provides an excellent locale for evaluating rifting in regions with minimal volcanism. Recent magmatism in the Western Rift is limited to four isolated volcanic provinces that initiated prior to or during the onset of faulting and basin formation (e.g., Ebinger et al., 1989; Furman, 2007). Tomographic imaging shows that eruptive centers in the Miocene-Recent Rungwe Volcanic Province (RVP) are underlain by low-velocity zones in the uppermost mantle (e.g., Accardo et al., 2017; Grijalva et al., 2018; O'Donnell et al., 2013). Seismic studies of the spatially distributed Toro-Ankole Volcanic Province in Uganda found low crustal and upper mantle velocities beneath the rift basins and the volcanic province, with evidence for migration of melt and CO₂ and modification and thinning of the lithosphere (Jakovlev et al., 2013; Wölbern et al., 2012). Vp/Vs derived from receiver functions in the southern Tanganyika rift also suggests elevated temperatures and/or melt in the crust in some parts of the rift away from the volcanic centers at the surface (Hodgson et al., 2017). However, at larger scale, imaging beneath the Western Rift fails to detect pervasive slow upper mantle like that observed beneath the Eastern Rift (e.g., Adams et al., 2018; Hansen et al., 2012), where it has been associated with the broad low-velocity zone rising from the core-mantle boundary (e.g., French & Romanowicz, 2015). In detail, the thermal state and distribution of partial melt beneath the Western Rift, and implications for lithospheric weakening and rifting, is poorly known.

In this work, we present local-scale shear velocity imaging of the crust and upper mantle spanning the Malawi Rift in the southern Western Rift using the Study of Extension and maGmatism in Malawi and Tanzania (SEGMeNT) onshore/offshore broadband seismic array and nearby stations. By combining these images with forward models of shear velocity from temperature, grain size, melt content, and composition, we evaluate the lithospheric architecture, thermal state, and possible melt distribution beneath the rift basins, the adjacent volcanic province, and the surrounding rift flanks. These images provide new constraints on the mechanisms of lithospheric weakening and localization of extension in relatively magma-poor rift regions.

2. Tectonic Setting

The East Africa Rift System exhibits along-strike variations in extension rate from 1–6 mm/year (King et al., 2019; Stamps et al., 2018), along with significant variations in the amount and distribution of seismicity and volcanism (Figure 1a), which are thought to represent fundamental differences in how extension is accommodated (e.g., Craig et al., 2011; O'Donnell et al., 2016), at least at shallow levels. The Western Rift is characterized by major fault-bounded rift basins and abundant and deep seismicity, while major magmatic systems dominate the Eastern Rift and Main Ethiopian Rift (Figure 1a). The Malawi Rift forms the southernmost extent of the Western Rift. Like other Western Rift systems, the Malawi Rift is characterized by strong lithosphere with active and deep crustal seismicity (Craig et al., 2011; Ebinger et al., 2019; Yang & Chen, 2010), limited surface volcanism (Furman, 2007) and asymmetric border-fault-bounded half grabens with polarities that vary along the rift (e.g., Ebinger et al., 1987; Scholz et al., 1989). Lake Malawi (Nyasa) covers approximately 550 km of the rift axis.

At shallow depths, the Malawi Rift is made up of three border-fault-bounded basins: North, Central, and South (Scholz et al., 2020; Figure 1b). Modest extension has occurred in this system, with cumulative crustal stretching based on flexural models of basin and flank morphology estimated at <20% (Ebinger et al., 1991). Thick (>5km) Neogene-to-recent sedimentary packages (Accardo et al., 2018; Shillington et al., 2020; Scholz et al., 2020) occur within both the North and Central Basins associated with significant offset on the basin-bounding border faults. Deep seismicity implies that the border fault continues to the base of the crust (Ebinger et al., 2019). At present, the lake reaches depths of nearly 700m, with the deepest portions localized adjacent to major basin-bounding faults in the North and Central Basins (Lyons et al., 2011).

The prerift continental lithosphere was constructed via a series of Proterozoic orogenies, including the Ubendian (~2,300–1,800 Ma), the Irumide (~1,350–950 Ma), and the Mozambique (~900–450 Ma; e.g., Fritz et al., 2013, and references therein). The Proterozoic orogens envelope Archean cratons (Figure 1c), and seismic tomography indicates thick lithosphere (>160 km) across the entire region (Fishwick, 2010). The North and Central Basins appear to lie within the abutting orogenic belts, with the structural sutures associated with them likely masked by the overlying Lake Malawi (Figure 1c). Following the last structural assembly during the Pan African, the SW-NE striking Ruhuhu and Maniamba extensional basins formed in the

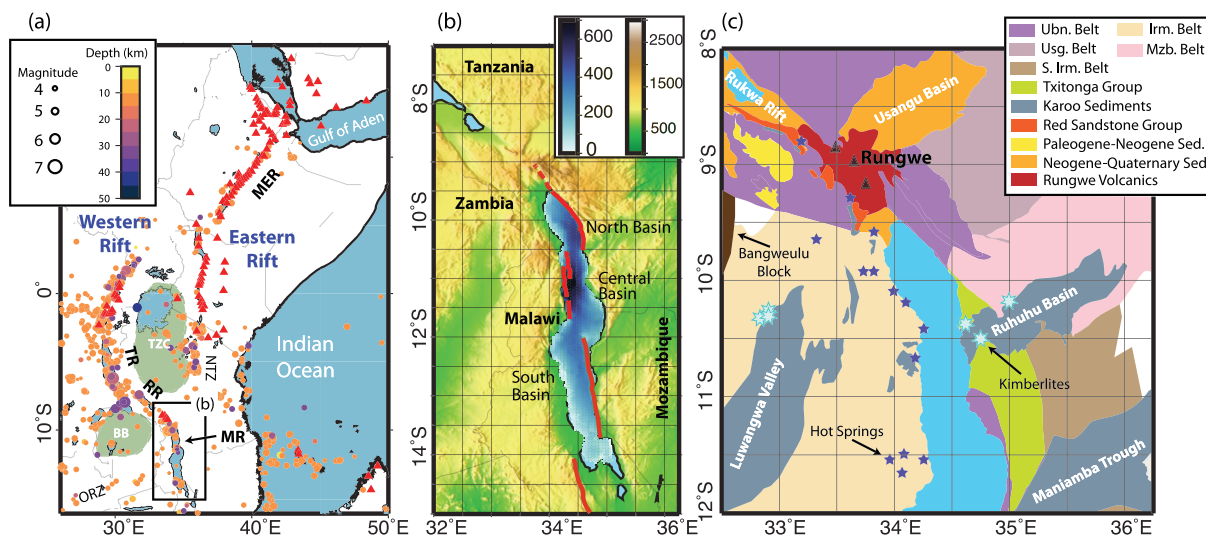


Figure 1. (a) Distribution of seismicity ($M_w > 2.5$ since 1970 from the International Seismological Centre catalog) and Quaternary-recent volcanoes along the East African Rift System from Smithsonian Global Volcanism Program (red triangles); TZC: Tanzanian Craton, BB: Bangweulu Block, MR: Malawi Rift, RR: Rukwa Rift, TR: Tanganyika Rift, NTZ: Northern Tanzania Divergence Zone, ORZ: Okavango Rift Zone, MER: Main Ethiopian Rift. The NTZ represents the southern continuation of the Eastern Rift and the ORZ represents northern continuation of the Southwestern Rift. (b) Topographic and bathymetric map of the Malawi Rift with locations of basin-bounding border faults shown in red. North, Central, and South Basins are indicated. Bathymetry from Lyons et al. (2011); scales are in meters. (c) Simplified geologic map of the North and Central Basins of the Malawi Rift highlighting the intersecting Proterozoic mobile belts; Ubn: Ubendian, Usg: Usagaran, Irm: Irumide, S. Irm: Southern Irumide, Mzb: Mozambique (Fritz et al., 2013). Volcanoes in the Rungwe Volcanic Province are marked (black triangles).

Late Paleozoic as a part of the broader Karoo rifting (Wopfner, 2002). The Ruhuhu Basin, which is situated at the juncture between the North and Central Basins, outcrops on both sides of Lake Malawi and appears to continue beneath the lake (Accardo et al., 2018; Figure 1c). The NW-striking basins between Malawi and Tanganyika, including the rift beneath the RVP, also formed during the Karoo episode (e.g. Wopfner, 2002).

The RVP sits at the northern end of the Malawi Rift, separating it from the Rukwa Rift, and it may overlie Karoo and Palaeogene rift basins (e.g., Accardo et al., 2018; Roberts et al., 2012). Magmatism in the RVP initiated by 19 Ma (Mesko, 2020) and possibly as early as 25 Ma (Roberts et al., 2012). The age of rift basins in the Western Rift is poorly known, but the ages of Rungwe volcanism suggest that volcanism may have preceded the estimated onset of faulting along the Livingstone border fault bounding the North Basin at ~8.6 Ma (Ebinger et al., 1989) and to renewed subsidence in the Rukwa Rift at 8.7 Ma (Hilbert-Wolf et al., 2017). Active magma reservoirs are thought to be present beneath parts of the RVP (Fontijn et al., 2012). Thermobarometry of mafic melts point to a relatively shallow depth of melting beneath the RVP (<110 km) and ambient to moderately elevated mantle potential temperatures ($T_p \sim 1199\text{--}1372^\circ\text{C}$; Class et al., 2018; Mesko, 2020). However, geochemical studies have found elevated $^3\text{He}/^4\text{He}$ in lavas and hot springs associated with the RVP (e.g., Hilton et al., 2011), suggesting the influence of a mantle plume in producing the volcanism.

SEGMeNT enables high-resolution constraints on faulting and rift-basin structure and evolution (Accardo et al., 2018; Ebinger et al., 2019; Scholz et al., 2020; Shillington et al., 2020), crustal and lithospheric architecture (Borrego et al., 2018; Hopper et al., 2018), and crust and mantle lateral heterogeneity and anisotropy (Accardo et al., 2017; Grijalva et al., 2018; Tepp et al., 2018). These studies provide refined images of a circular low-velocity region associated with the RVP within the uppermost mantle (Accardo et al., 2017; Adams et al., 2018; Grijalva et al., 2018). Mantle flow in the asthenosphere is inferred to be dominantly NE-SW south of the RVP, where increased complexity of the anisotropy may reflect a perturbation in mantle flow related to dynamics beneath the volcanic center (Tepp et al., 2018). North of the RVP in the Rukwa-Tanganyika Rift, anisotropy is rift parallel (NW-SE). Moho depths across the region range from 31–49 km, with variability in crustal thickness around the rift largely associated with different Proterozoic terranes (Borrego et al., 2018). Clear thinning of the crust is not observed along the rift flanks (Borrego

et al., 2018), suggesting that crustal thinning associated with recent extension is predominantly localized beneath the rift axis (Accardo et al., 2018). Mantle lithosphere thinning appears to be much stronger than crustal thinning, spanning ~100km across both the North and Central Basins (Hopper et al., 2018).

3. Data and Methods

3.1. Rayleigh Wave Phase Velocities for Malawi Rift

We construct a 3-D shear velocity model for the northern Malawi Rift region using the ambient-noise (9–20s) and teleseismic (25–100s) Rayleigh wave phase velocity data set of Accardo et al. (2017). This data set utilized both onshore and lake-bottom instruments from the SEGMeNT array (Shillington et al., 2016), the nearby TANGA14 array (Hodgson et al., 2017; Lavayssi  re et al., 2019), and three Africa Array stations (Nyblade, 2007), a total of 72 intermediate and broadband stations. Teleseismic Rayleigh wave phase velocities were measured using the Automated Surface-Wave Measuring System of Jin and Gaherty (2015), which leverages the coherency in surface wave trains recorded on nearby stations to robustly determine phase and amplitude information that are then plugged into a Helmholtz tomography algorithm (Lin & Ritzwoller, 2011). Phase velocity from ambient noise-derived Rayleigh waves was determined using the frequency domain cross-spectrum method of Menke and Jin (2015) and ray-theory tomography (Jin et al., 2015). Resulting maps of phase velocity have a grid spacing of 0.2° (~22km), spanning an irregular region that extends from the central Malawi Rift to the south, up to the southeastern end of Lake Tanganyika. Here we utilize the portions of the phase velocity map centered on SEGMeNT, namely, east of 32°E, which is covered by relatively closely and regularly spaced seismic instruments (Figure 2). Resolution tests suggest that the data resolve structural variations with length scales ~70km and larger at ambient noise periods across the entire SEGMeNT array (Accardo et al., 2017; Figure S1 in the supporting information). At longer periods, the low root-mean-square variance in phase velocity derived from different earthquakes (<0.03km/s) suggests that the final average phase velocity variations are well resolved within the SEGMeNT array (Accardo et al., 2017). Events were well distributed in back azimuth (Accardo et al., 2017), and phase velocity inversions both neglecting and including terms for azimuthal anisotropy generally produced isotropic phase velocity maps that were consistent within error. Here we utilize phase velocity maps derived from the isotropic inversion. Overall, average phase velocities are similar to the average found in previous studies of the Western Rift (O'Donnell et al., 2013) but are up to 5% slower than phase velocities representative of the Archean Tanzanian Craton (TZC) (O'Donnell et al., 2013) and over 5% faster than phase velocities of the magmatic Main Ethiopian Rift (Accardo, 2018; Figure 3).

3.2. Shear Velocity Inversion for Malawi Rift

To estimate 3-D variations in crust and mantle shear velocity across the region, we follow the procedure utilized in Jin et al. (2015). We invert dispersion curves retrieved from maps of phase velocity at each grid point for models of 1-D shear velocity using the *surf96* program (Herrmann, 2013). This is a linearized least squares inversion method that implements differential damping to enforce smoothness by seeking to minimize the differences in model changes within each individual layer. To minimize biases resulting from choices in the starting model and provide estimates of model uncertainty, we invert a family of starting models for each grid point. Starting models consist of sediment, crust, and mantle layers that are each constructed with node spacings of 1, 6, and 10 km, respectively. We guide the construction of initial models for each location using a priori information on water depth in Lake Malawi (Lyons et al., 2011) and sediment thickness from seismic reflection and wide-angle refraction data (Accardo et al., 2018) and crustal thicknesses from receiver function studies (Borrego et al., 2018; Hodgson et al., 2017). Figure 2 shows a spline surface fit to point estimates of Moho depth used for constraining crustal thickness in the inversion. This surface does not capture abrupt station-to-station fluctuations observed in the receiver-function results, but it effectively characterizes within error the smooth variations in Moho depth at wavelengths associated with the surface wave velocities. We introduce Gaussian-distributed perturbations to individual layer velocities and velocity boundaries (sediment/crust and crust/mantle boundaries) through a Monte Carlo approach to create 100 unique starting models. We allow variations in individual layer velocities within the crust and mantle to provide a more varied family of starting models. Table 1 details the allowed perturbations to the parameters of interest. Models extend to 400 km depth but are constrained toward iasp91 below 225 km. We fit the full phase velocity data set out to periods of 100 s, but the longest periods only constrain the

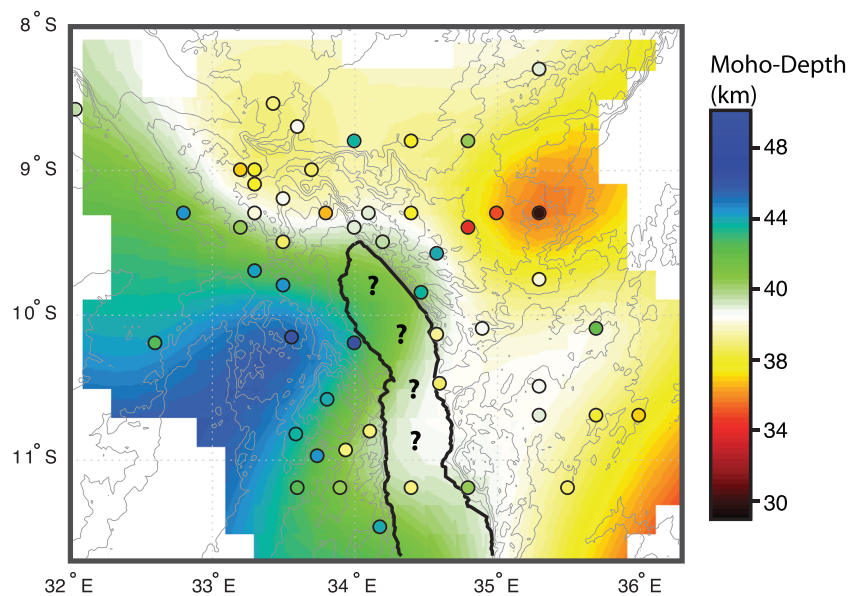


Figure 2. Smooth model of Moho depth beneath Malawi Rift region, derived from a surface-spline fit to point receiver-function estimates of Hodgson et al. (2017) and Borrego et al. (2018). Circles represent the stations, with symbol color providing the mean depth estimate. Question marks indicate region of poor constraints beneath the rift basin from onshore receiver function results. Surface is constructed to capture the smooth regional variation for input into the surface-wave models, and cannot capture abrupt fluctuations.

average velocity at depth due to long spatial wavelengths that are of the same order as our $\sim 300 \times 300$ km array. As a result, models show very little spatial variation below ~ 150 -km depth. To avoid misinterpretation of this near constant velocity at larger depths, we limit our interpretation to less than 135-km depth. This choice is also consistent with the peak sensitivity of our data set (Figure 4).

Phase velocity sensitivity kernels (Figure 4) are calculated using a normal-mode formalism and account for the presence of a water layer for grid points that lie over 50% within the lake. Uncertainties in the dispersion observations are derived from the phase velocity inversions and are generally <0.03 km/s. The synthetic phase velocity calculation incorporated the effect of physical dispersion, assuming a frequency-independent Q model that smoothly transitions from a low attenuation lithosphere ($Q = 180$) above 120-km depth to a moderately attenuating asthenosphere ($Q = 80$), and a reference frequency of 35 mHz. Ignoring the effect of physical dispersion would result in shear velocities that are 0.7% slower than our model in asthenospheric regions. For each individual inversion, we employ relatively weak damping in the surf96 inversion, and the resulting models generally fit the data to within error (normalized $\chi^2 \sim 1$). Due to trade-offs inherent in surface wave sensitivity, these weakly damped models may have significant variability with depth, with standard deviations in velocity of any given depth spanning 0.07–0.12 km/s through most of the crust and upper mantle (Figure S2). We discard models with the largest misfits ($>20\%$ above the average misfit, which usually corresponds to $<10\%$ of the 1-D models) and calculate the mean of the remaining models as the representative 1-D model for each grid point. These average 1-D models vary smoothly with depth and laterally, effectively characterizing variations in velocity structure required to fit the individual dispersion curves. The mean velocity profiles are quite robust with respect to the choice of cutoff for misfit; increasing the cutoff to include only

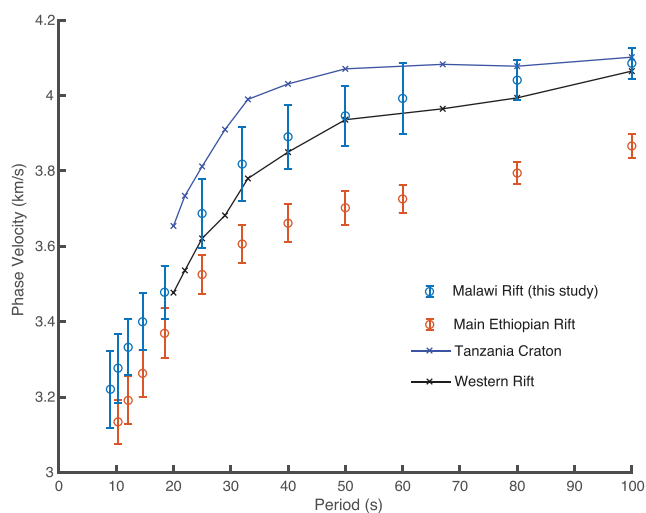


Figure 3. Average regional dispersion curve for the Malawi Rift (blue circles) compared to other tectonic domains in East Africa: Main Ethiopian Rift (red circles), measured by Accardo (2018) using the same algorithm applied here; Tanzania Craton (dark blue curve) and western branch of the EAR (black curve) from O'Donnell et al. (2013). One standard deviation of variance within Malawi and Ethiopia regions are shown and reflect the spatial variability of velocity within the regions.

Table 1
Allowed Perturbations to the Starting Models for the Shear Velocity Inversion

Parameter	Allowed perturbation
Sediment velocity	$\pm 10\%$
Crustal velocity	$\pm 10\%$
Mantle velocity	$\pm 10\%$
Sediment thickness	$\pm 1 \text{ km}$
Moho depth	$\pm 5 \text{ km}$

Note. Sediment thickness and Moho depth are applied to location specific starting models that incorporate constraints from Accardo et al., 2018 and Figure 2.

the best 50% of the models (rather than ~90%) results in nearly identical velocity profiles and associated variance. This suggests that uncertainty on these mean velocity profiles is significantly smaller than their standard deviation, generally $<0.02 \text{ km/s}$, but to be conservative we report the standard deviation values here. Vertical resolution is of order 10 km within the crust, increasing to ~20 km in the shallow mantle. Figure 5 shows examples for several locations in our model, showing the suite of starting models and resulting models and forward modeled dispersion curves. We construct our final 3-D model by combining the 1-D shear velocity models at each $0.2^\circ \times 0.2^\circ$ grid point sampled by the phase velocity data set. No lateral smoothing is applied.

4. Results and Velocity Interpretation

Our final Vs model provides a 75% variance reduction to the fit of the phase velocity observations compared to a mean Vs model for the region. As noted above, we utilize the standard deviation of the model ensembles to provide conservative estimates of uncertainty in shear velocity (Figure S2), which are typically $<0.10 \text{ km/s}$. Standard deviations are highest in the depth ranges of the sediment-crust and crust-mantle interfaces due to the limited ability of surface waves to constrain sharp jumps in velocity structure, and so we avoid detailed interpretation close to those boundaries. Our results are largely consistent with the shear velocity model of O'Donnell et al. (2013), though the model presented here exhibits more lateral variation due to the increased spatial resolution of this data set. They are also consistent with body wave imaging from the SEGMeNT study (Grijalva et al., 2018).

Figures 6 and 7 show depth and cross-section slices through our final shear velocity model for the Malawi Rift. Shear velocities vary laterally by up to 5% in the crust and up to 8% in the mantle, with the slowest velocities correlating with the RVP and fastest velocities observed beneath the Proterozoic-age Southern Irumide belt east of the Central Basin (SE Flank, Figure 6d). Mantle velocities associated with cold, depleted continental lithosphere ($V_s \sim 4.6\text{--}4.7 \text{ km/s}$) extend to the base of the model beneath the southeastern flank of the rift, while velocities likely corresponding to asthenosphere ($V_s < 4.4 \text{ km/s}$; Faul & Jackson, 2005; Nettles & Dziewonski, 2008) are found immediately beneath the Moho beneath the RVP, at depths greater

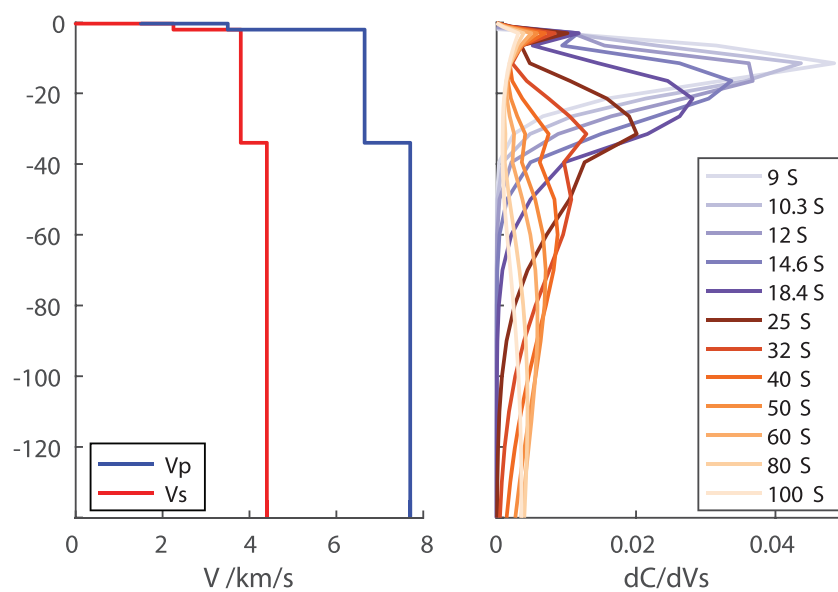


Figure 4. Sensitivity kernels for Rayleigh wave phase velocity with respect to isotropic shear velocity in upper 140 km, for the period band utilized here. Model includes thin water and sediment layers, in addition to constant-velocity crust and mantle. The longest-period band (100 s) peaks near 140 km and largely constrains only average velocities below this depth.

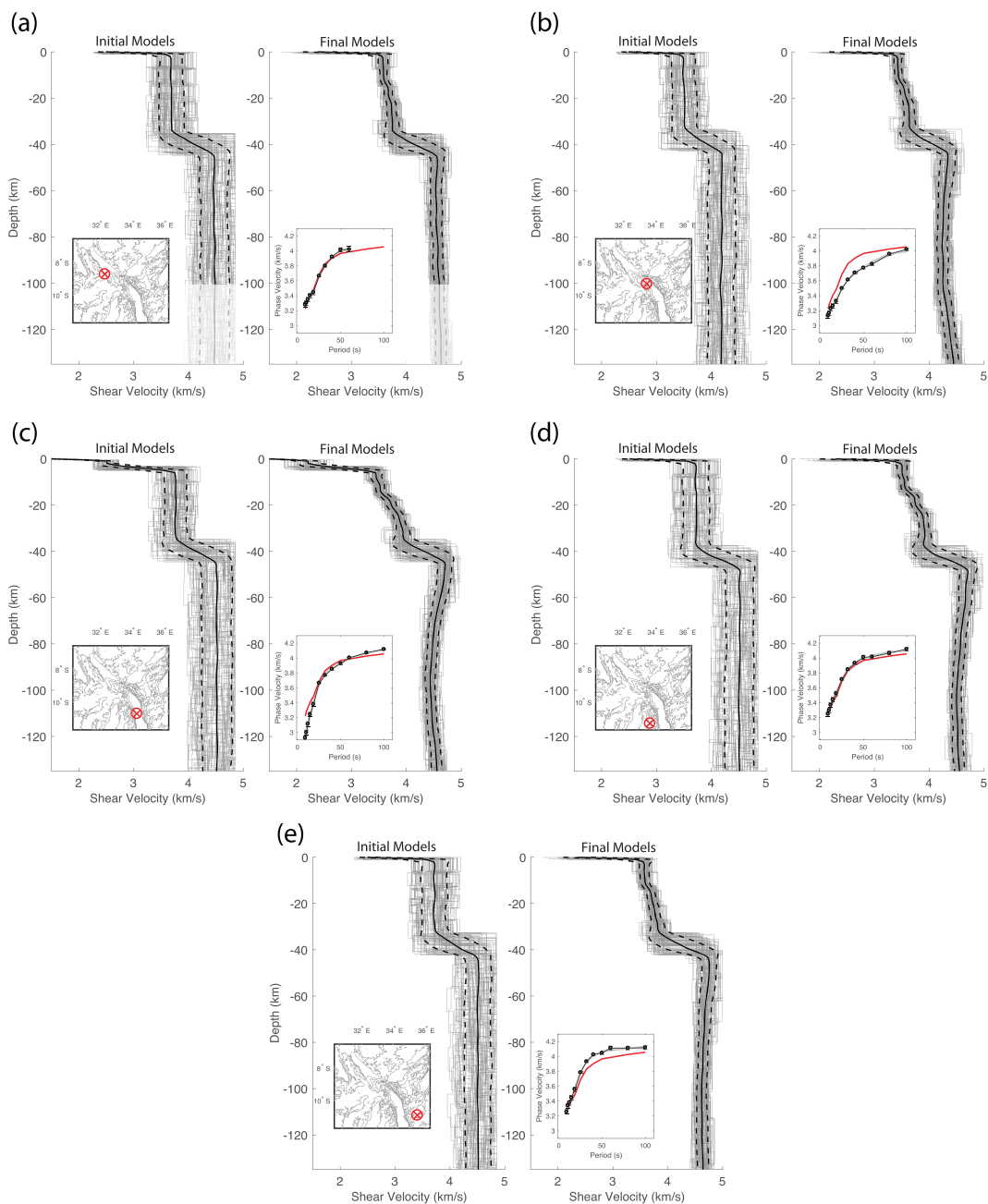


Figure 5. (a–e) Examples of 1-D shear velocity inversions at several locations. The left panel of each subplot shows the suite of initial models with an inset plot showing topography contours (gray) and the location of the profile within the study region (red circle). The right panel shows the suite of final models and the inset plot shows a comparison between the suite of predicted phase velocity dispersion curves (gray), observed phase velocities (black symbols with error bars and black curve), and the mean dispersion curve for the entire study region from Figure 3 (red curve). Error bars on phase velocity observations represent one standard deviation, and they are similar to the symbol size. The average (solid) and one standard deviation (dashed) of the initial and final models are shown by the thick black lines. Note that locations NW of the RVP like in (a) only have phase velocity measurements out to 60 s.

than ~ 70 km beneath the rift axis and the associated border faults, and deeper than ~ 110 km on the western side of the rift axis (Figures 7 and 8). Moving south down the rift axis from the RVP, velocities generally increase, with shallow mantle characterized by shear velocities intermediate between stable lithosphere and asthenosphere (4.4 and 4.5 km/s, Figure 7b). While surface waves generally cannot distinguish between abrupt discontinuities and transitions spread over ~ 20 - to 30-km depth and thus do not provide unambiguous constraints on lithospheric thickness (e.g., Fishwick, 2010; O'Donnell et al., 2013), the transition from

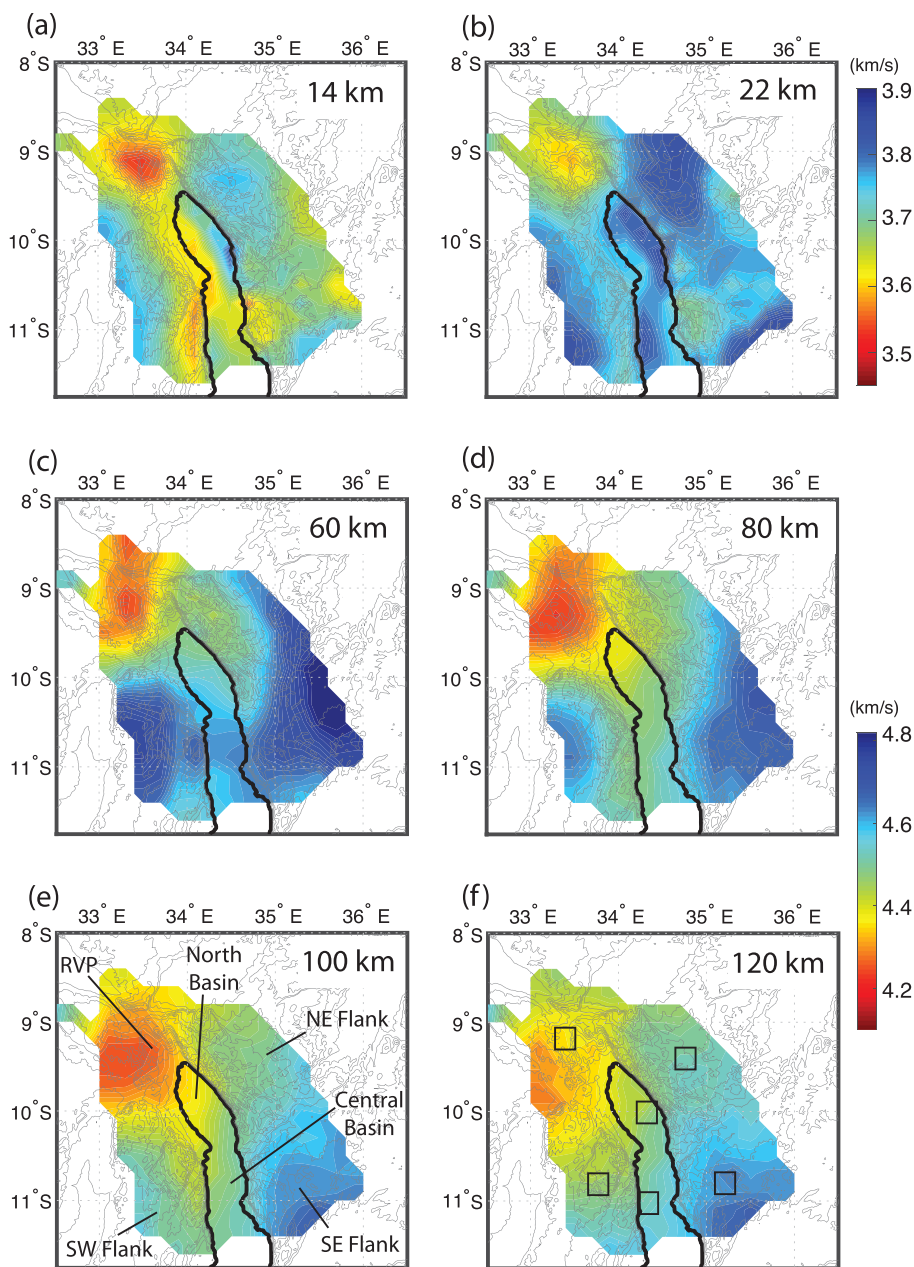


Figure 6. Map view of depth sections through the mean shear velocity model. (a, b) Sections through the mid and lower crust (16 and 22 km). (c-f) Mantle slices at 60, 80, 100, and 120 km. Gray lines show topography contours, and the heavy black line represents the shoreline of Lake Malawi. Regions described in the text are labeled in (e). Locations of representative 1-D model averages presented in Figure 8 are indicated by open squares in panel (f). Color scales differ for crust and mantle depths.

clearly lithospheric (>4.6 km/s) to likely asthenospheric (<4.4 km/s) velocities generally occurs at depths that correspond closely to the depth of a strong negative velocity gradient observed in scattered-wave images (Hopper et al., 2018).

Our model parameterization includes the crust for completeness, but it is not the focus of this study. The upper crust is highly heterogeneous, with surface exposures of metamorphic terranes, young lavas, and broad deep, fault-bounded sedimentary basins, with abrupt transitions between them. Such structures are not well described by a $0.2^\circ \times 0.2^\circ$ model, and we leave detailed discussion to other analyses (Accardo et al., 2018; Scholz et al., 2020; Shillington et al., 2020). At middle to lower crustal depths (16, 22 km), the

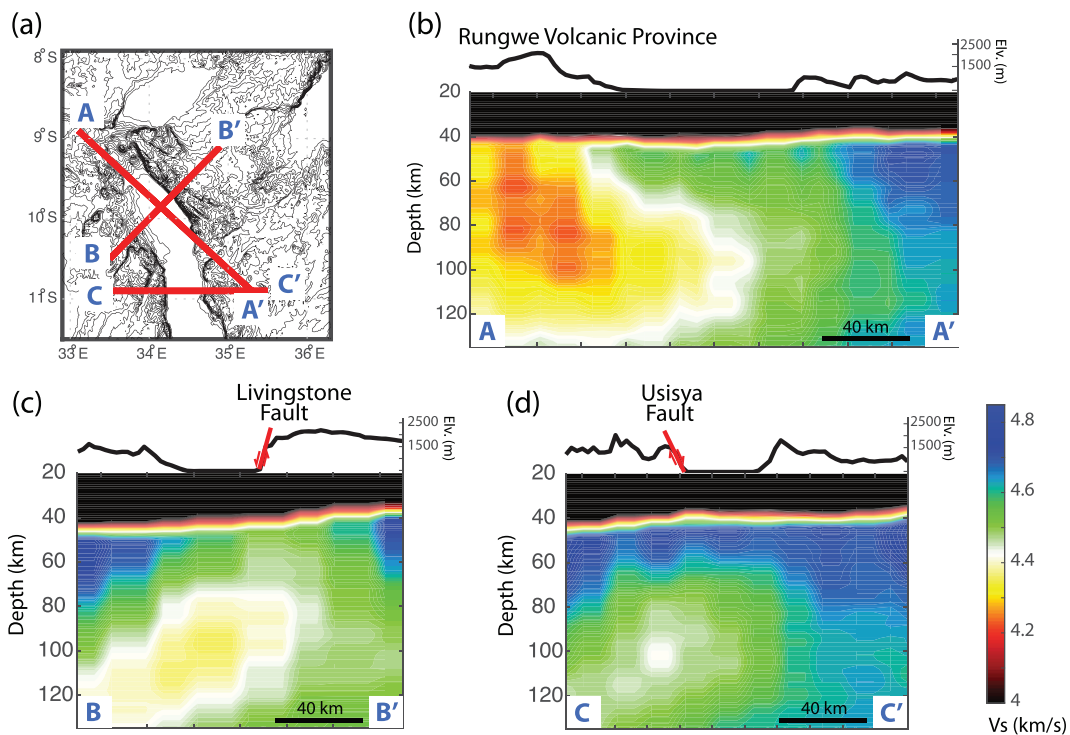


Figure 7. The 2-D cross sections through the final velocity model with topography shown on top with a vertically exaggerated scale. Locations of interest are labeled along with fault motions for the two border faults. (a) Location map. (b) Along-axis cross section through Rungwe Volcanic Province and North Basin of Malawi Rift. (c) Cross section through North Basin of Malawi Rift. (d) Cross section through Central Basin of Malawi Rift.

shear velocity model captures a localized, low-velocity anomaly beneath RVP with velocities in the range of 3.5–3.6 km/s, surrounded by crust that shows small-amplitude, large-scale variations in the range of 3.7–

3.9 km/s; Figures 6a, 6b, and 8). The anomalously slow (3–5%) velocities beneath RVP likely reflects both the recent volcanism, as well as the contribution from underlying unknown thicknesses of Karoo, Cretaceous, Paleogene, and Miocene-Recent sediments that are exposed in fault-bounded outcrops along the western, flexural margin of the North Basin (Figure 1c; e.g., Ebinger et al., 1989; Roberts et al., 2012) and thought to continue beneath the rift (Accardo et al., 2018). Inversion tests suggest that the low velocities through the mid and lower crust are required even if a thicker sediment-influenced layer is incorporated in the upper crust. At 16-km depth (Figure 6a), a linear slow trend extends along the western shore of the lake that correlates with extended and faulted rift hanging wall along the North Basin. However, the adjacent high-velocity contrast is highly correlated with the deepest portions of the rift basins and suggests that perhaps the abrupt basin transitions are not well captured by a smooth model. Overall, the crustal velocities are consistent with those inferred for the region from receiver functions and are within the expected range for ancient continental crust in Africa (Borrego et al., 2018).

Below, we discuss several of the primary observations resulting from our velocity model of the Malawi Rift.

4.1. RVP

Low velocities are clearly observed beneath the RVP at crust and upper mantle depths. Within the mantle, a minimum velocity of

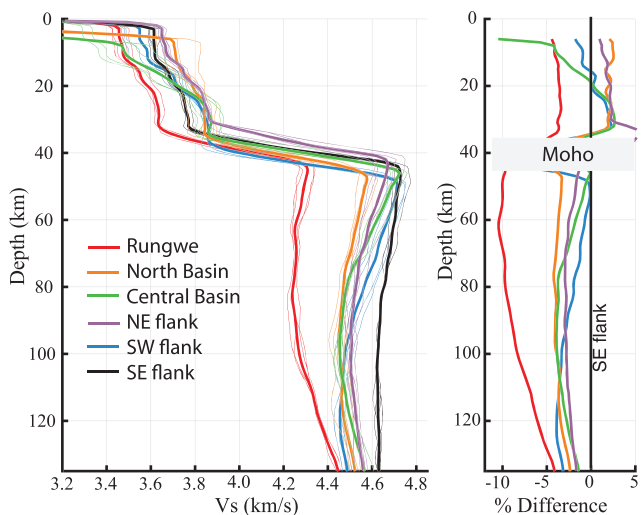


Figure 8. (a) Comparison of 1-D average Vs profiles for six regions discussed in the text (locations shown in Figure 6f). For each set of models, the heavy lines represent the mean of the vertical Vs profiles at four adjacent points in the model, shown as the bracketing thin lines. Red: Rungwe Volcanic Province; orange: North Basin; green: Central Basin; violet: northeastern flank; blue: southwestern flank; black: southeastern flank. (b) Percent shear velocity difference between the presumably unmodified southeastern flank and the other regions.

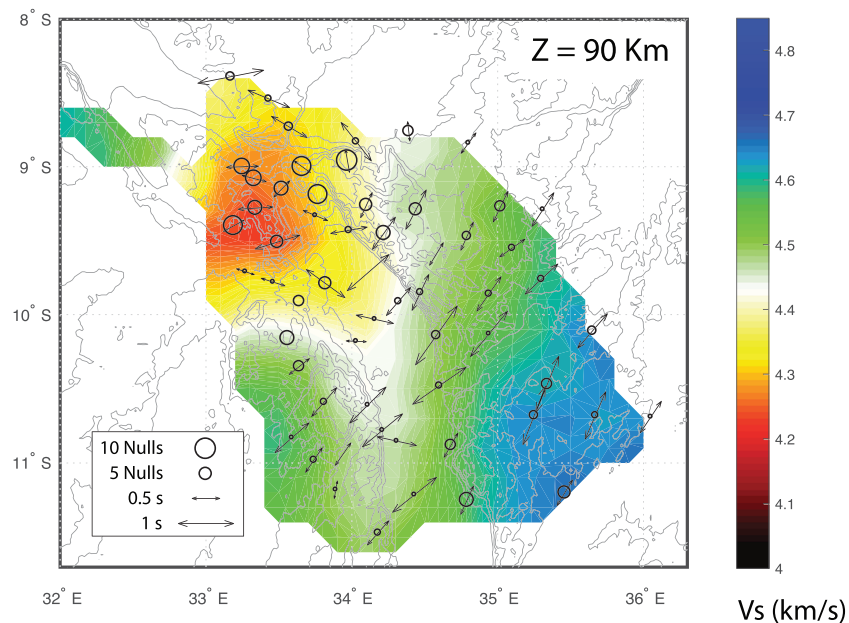


Figure 9. Comparison between velocity structure at 90 km from this study and the station-average shear wave splitting results of Tepp et al. (2018). The length of each vector indicates the average splitting time, and the direction of each vector indicates the fast direction of anisotropy. Circles indicate stations where null observations of splitting were reported, and the size of the circle represents the number of null observations.

~4.25 km/s occurs in this anomaly at ~80-km depth (Figure 8), though pronounced low velocities (<4.3 km/s) extend from the Moho to at least ~135 km. Previous studies have imaged the velocity anomaly associated with the RVP from surface waves (e.g., O'Donnell et al., 2013) and body waves (Grijalva et al., 2018; O'Donnell et al., 2016) extending to depths of ~120 and >150 km, respectively. At 135 km, the velocity anomaly associated with the RVP remains slower than the rest of the study region, indicating that the anomaly likely extends deeper than we can resolve. The edge of the RVP feature is relatively sharp in map view at crustal (Figures 6a and 6b) and shallow mantle (Figures 6c and 6d) depths constrained by shorter-period data, and it does not continue northwest into the Rukwa Rift (Accardo et al., 2017). It has a diameter (~100–150 km at 80-km depth). These observations match well with the limited spatial extent of complex azimuthal anisotropy mapped by shear wave splitting (Tepp et al., 2018; Figure 9).

4.2. Western and Eastern Rift Flanks

We define the regions outside of Lake Malawi and the RVP as the southwestern flank, the southeastern flank, and the northeastern flank (Figure 6d). The highest-velocity mantle is observed in the southeastern flank, where $V_s > 4.6$ km/s from the Moho to beyond the base of the model (>135 km) indicates intact, cold continental lithosphere. The southwestern flank is characterized by high velocities (4.7 ± 0.1 km/s) just below the Moho, which then transition to lower (possibly asthenospheric) velocities by ~110-km depth. The northeastern flank is slower than either of the southern flanks, particularly at shallow depths (50–80 km) where velocities are <4.5 km/s. The relatively slow velocities continue to depths of ~110 km, where this region has similar velocities to those of the southwestern flank. These velocities are intermediate between those expected for continental lithosphere and underlying asthenosphere (i.e., Faul & Jackson, 2005), and we interpret them as indicative of mantle that has been modified through thermal or metasomatic processes, as discussed below. The northeastern flank is also characterized by slightly thinner crust than the other rift flanks (Borrego et al., 2018; Figure 2). While there is some trade-off between the thin crust and slow mantle velocities in this region, inversion tests suggest that the slow (modified) mantle velocities in the northeast cannot be eliminated by assuming a crustal thickness comparable to the other flanks. The seismic properties of terranes surrounding the rift from this study are consistent with body wave imaging from the SEGMeNT study (Grijalva et al., 2018) and with results from regional body wave and surface wave studies (e.g., O'Donnell et al., 2013, 2016), though the latter have lower spatial resolution.

4.3. Malawi Rift Axis

We observe intermediate velocities (~4.45–4.55 km/s) suggestive of modified mantle lithosphere and shallow asthenosphere beneath the rift axis, with velocities generally decreasing to a minimum velocity of ~4.40 km/s near ~80- to 100-km depth (Figure 7). The significant lithospheric thinning implied by the shallow low-velocity zone is consistent with that inferred from scattered wave imaging (Hopper et al., 2018). The cross sections (Figure 7) illuminate a distinctive asymmetry in across-rift structure, with the low velocities centered beneath the rift axis and footwall escarpments of both the North and Central Basins. In the North Basin, the high-velocity lithosphere of the SW flank abruptly transitions to thinner, intermediate-velocity lithosphere that has a minimum velocity beneath the Livingston border-fault escarpment and extends over 100 km to the northeast. However, at 80- to 100-km depth, where the minimum in $V_s(z)$ of 4.4 km/s likely defines shallow asthenosphere, the lowest velocities are centered beneath the rift axis. In the Central Basin, the thick, high-velocity lithosphere of the SE flank transitions at the lake shore into a thinned zone of lower velocities that reach a minimum beneath the Usisya fault footwall west of the lake. Velocities are slower beneath the axis of the North Basin (minimum $V_s < 4.4$ km/s) than the Central Basin (Figure 7), perhaps due to the thermal influence of the RVP, although it is difficult to rule out a degree of smearing of low velocities from the RVP into the North Basin (Figure S1). Overall, the lateral variations in mantle shear velocities are consistent with the *P* and *S* body wave tomography images of Grijalva et al. (2018), in which they see the strongest anomaly, excepting the RVP, to be centered beneath the lake and extending into the footwall of the North Basin. They also observe a more modest reduction of velocities centered along the western lakeshore in the Central Basin.

5. Discussion

A coherent portrait of the lithospheric architecture and thermal state emerges from the shear velocity modeling, providing a means to characterize the regional framework and assess the processes associated with Cenozoic rifting. We image thick, high-velocity structure beneath the SE flank, and based on surface geology (Figure 1), high shear velocity (>4.6 km/s), and thickness (>130 km), we interpret this flank to represent unmodified Proterozoic lithosphere. Compared to this relatively unmodified flank, we interpret the slower velocities and locally thinned lithosphere to result from Cenozoic rifting and RVP magmatism. The characteristics of the velocity structure provide important constraints on the geometry of lithospheric extension, and the underlying thermal and mechanical processes enabling localized weakening in strong cold cratonic lithosphere.

5.1. Properties of Proterozoic Terranes

The Irumide and Southern Irumide belts (e.g., Fritz et al., 2013) are characterized as a high-velocity lid in the southwest and southeast portions of the model, respectively, which we interpret as cold Proterozoic lithosphere (Ebinger et al., 1991; Nyblade & Pollack, 1993). Both regions exhibit shear velocities of 4.6 to 4.7 km/s, extending to ~90-km depth to the west beneath the Irumide, and to over 130-km depth to the east beneath the Southern Irumide (Figure 7). These depths are compatible with lithospheric thickness estimates from *S* to *P* imaging (Hopper et al., 2018), and electromagnetic imaging of upper mantle conductivity suggest similar thickness variations of a resistive lithospheric layer in both regions (Sarafian et al., 2018). The variations in the thickness of the high-velocity lid could either represent lateral heterogeneity in the prerift structure or synrift modification of lithosphere on the western side of the rift. Larger-scale tomographic imaging (O'Donnell et al., 2013) indicates lithospheric thickness of at least 120 km across the broader region, but it also shows slower, thinner lithosphere along the western flank of Lake Malawi. This flank of the Malawi Rift shows evidence of Triassic and later extension that extends west to the Luangwa rift (Figure 1c). We interpret the southwestern flank to be modestly thinned by multiple stages of rifting, while the southeastern flank beneath the Southern Irumide remains unmodified.

To the northeast, upper mantle velocities beneath the Usagaran terrane and Usangu rift are 5% slower than other regions surrounding the rift (Figure 6c). This area also has distributed high topography (>2,200 m) and anomalously thin crust (<34 km) compared to other parts of the study region outside the rift (Figure 2; Borrego et al., 2018). Taken together, these factors suggest thermochemical modification of the northeastern flank. Such modification may be enhanced here due to the proximity to the RVP or related to its location

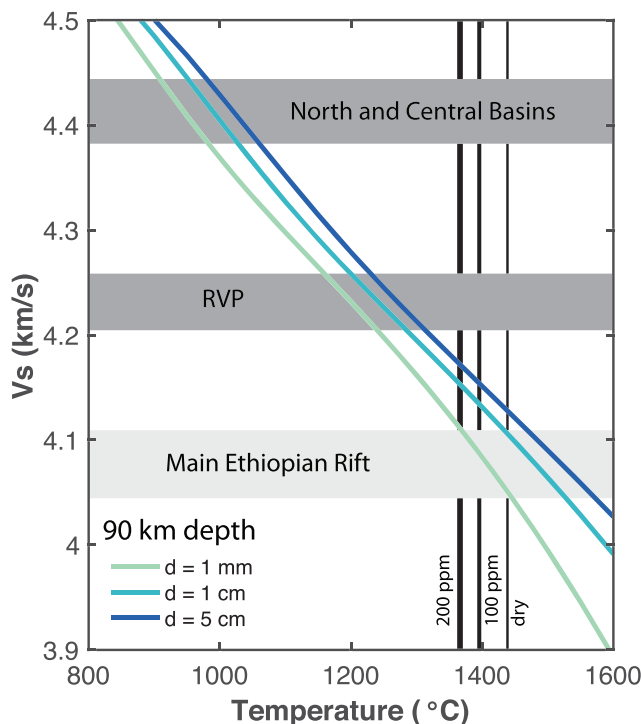


Figure 10. (a) Predicted shear velocity versus temperature at a depth of 90 km for melt-free olivine at three different grain sizes using the anelastic model of Jackson and Faul (2010; solid lines). Vertical black lines correspond to solidi for dry and modestly wet (100 and 200 ppm H_2O) conditions (Katz et al., 2003). The lowest observed shear velocities in the 80- to 100-km-depth interval from the North and Central Basins and the Rungwe Volcanic Province are shown with the dark gray bands; the velocities in the Malawi basins and the RVP are consistent with subsolidus conditions. In contrast, the central Main Ethiopian Rift (light gray) likely requires partial melt to explain the low shear velocities found in other studies (Accardo, 2018; Gallacher et al., 2016).

within the region of diffuse deformation between the Eastern and Western Rifts (e.g., Adams et al., 2018; Mulibo & Nyblade, 2016).

5.2. Lithospheric Modification below the Malawi Rift

Mantle shear velocity structure beneath both the North and Central Basins of the Malawi Rift shows two clear effects of Cenozoic extension. First, the cross sections (Figure 7) suggest an effective thinning of the lithospheric mantle, bringing asthenosphere-like velocities to depths of 80–100 km beneath the rift axis. Second, velocities within the thinned lithosphere are 1–5% slower than the adjacent SE flank (Figure 8), suggesting that the lithosphere beneath the rift axis has been thermally or chemically altered. Here, we focus on the absolute shear velocities associated with the system to better constrain the modification process.

Although the mantle shear velocities beneath the active portions of the Malawi Rift are lower than the eastern flank, they are very high compared to more volcanically active portions of the EARS. This is true both for the modified lithosphere in the system, as well as the underlying asthenosphere. Shear velocity profiles through the slowest portions of the North and Central Basins (Figure 8) have minimum shear velocities of 4.40–4.45 km/s, which are much higher than velocities of <4.1 km/s observed at similar depths beneath the Main Ethiopia rift (Accardo, 2018; Gallacher et al., 2016). Based on the experimental constraints of Jackson and Faul (2010), the relatively high velocities observed beneath the Malawi Rift preclude substantial volumes of partial melt. Assuming a reasonable range of grain size (0.1–5 cm), the velocities imply in situ temperatures of ~950–1050°C at ~80- to 100-km depth (Figure 10). Alternatively, an empirically constrained model of the velocity-temperature relationship suggests that a velocity of 4.4 km/s corresponds to temperatures at ~100-km depth of 1150–1200°C (Goes et al., 2012). Both of these temperature estimates are well below the expected solidus for dry or damp peridotite melting (Katz et al., 2003; Figure 10), an inference consistent with shear velocity estimates from other regions where partial melt is evaluated (e.g., Gallacher et al., 2016; Goes et al., 2012; Rau & Forsyth, 2011).

It is difficult to isolate the specific mechanism(s) responsible for the reduction in mantle-lithosphere velocities beneath the rift valley. The slow anomalies are almost certainly in part due to thermal perturbation associated with mantle-lithosphere thinning. While simple scaling calculations suggest that a temperature perturbation in the asthenosphere would thermally conduct only ~10 km upward over an ~20-Myr time scale (Turcotte & Schubert, 2014), a thinning process that advects near-adiabatic temperatures to shallower depth would result in modest warming (and thus weakening) of the entire lithospheric column. Motivated in part by the spatial correlation between the Malawi Rift and the ancient subduction suture implied by the Ubendian belt (Boniface & Schenk, 2012; Fritz et al., 2013), Hopper et al. (2018) hypothesize a specific thermal advection process to weaken the lithospheric mantle and enable extension to initiate. They envision flux melting of volatile and pyroxene-rich components of the lithospheric suture occurring at relatively modest temperature and propagating upward via percolation or diking (e.g., Havlin et al., 2013), carrying heat with it via transport and subsequent freezing and release of latent energy. The thermal and metasomatic processes weaken the lithosphere, enabling strain localization in these weaker zones. The trigger for the initial melting could be a small increase in temperature at the base of the lithosphere, perhaps associated with the influx of plume material associated with regional volcanism (e.g., Ebinger & Scholz, 2012). Because the volume of fusible elements is finite, the volume of partial melting will be small if temperatures remain below the dry solidus, and the process can serve to weaken the lithosphere without producing substantial magmatism. From temperature alone, this process could reduce shear velocities in the mantle lithosphere by several

percent (Hopper et al., 2018). The reduction in velocities due to this thermal perturbation could be further enhanced by a compositional effect, with cooled pyroxenite and/or solidified silicic melts left behind in the shallow mantle due to inefficient melt extraction reducing the velocities relative to those expected for lherzolite (e.g., Gaherty & Dunn, 2007; Lizarralde et al., 2004). The shear wave velocities presented here suggest either that the volumes of melts are very small or that melt products that facilitated this weakening and modification are no longer in the system. The mantle lithosphere is substantially more thinned than the overlying crust (Hopper et al., 2018) suggesting a bottom-up rifting process enabled by only small and/or ephemeral amounts of magmatism.

The distribution of low velocities in the mantle lithosphere and asthenosphere are modestly asymmetric with respect to the overlying half-graben basins. Beneath the North Basin, the lowest lithospheric velocities are located along a projection of the Livingstone border fault (i.e., the footwall block), rather than being centered only under the rift axis. A similar pattern is observed in a *P* and *S* velocity models of this region derived from body waves (Grijalva et al., 2018). Beneath the Central Basin, the asymmetry is observed slightly deeper, where the minimum velocities observed in the asthenosphere are centered beneath the Usisya border fault. The asymmetry may partially result from isostatic adjustments driving rift-flank uplift during extension in strong lithosphere (e.g., Ebinger et al., 1991; Weissel & Karner, 1989). Our results have the opposite sense of asymmetry predicted by some dynamic models of rifting that include enhanced lithospheric thinning near the downdip end of the border fault beneath the hanging wall (e.g., Brune et al., 2014). However, the comparable patterns of low lithospheric and/or asthenospheric velocity and the overlying border fault systems in the crust, even as polarity reverses between the two rift segments, suggest a coupling between extension in the crust and mantle lithosphere. Many mature rifts and rifted continental margins exhibit substantial asymmetry (e.g., Hopper et al., 2003; Shillington et al., 2006), and our results suggest asymmetry throughout the lithosphere may be established early in the rifting process.

5.3. Nature of RVP

The most prominent feature in our model is the low-velocity anomaly in the upper mantle and crust associated with the RVP. The RVP represents a long-lived (up to ~24 Ma to Recent; Roberts et al., 2012; Mesko, 2020) magmatic province that may have initiated prior to the development of the Malawi Rift basins (e.g., Ebinger et al., 1989). The magma production rate is very slow, with a continuum of ages showing possible gaps in activity between ~17 and 11 Ma (Mesko, 2020), with the three active volcanoes built on edifices of earlier shield complexes (Fontijn et al., 2010). The low-velocity seismic anomaly is driven at least in part by the influx of heat via episodic magmatic intrusion and crystallization in both the crust (e.g., Till et al., 2019) and upper mantle (e.g., Goes et al., 2012). Previous results provide support for the presence of elevated temperatures and potentially melt in the crust. High surface heat flow (Branchu et al., 2005) and Bouguer gravity anomaly lows associated with Rungwe volcano (Ebinger et al., 1989) have been interpreted to suggest some shallow magma body within the crust. Receiver functions from stations in the RVP have high crustal *Vp/Vs* ratios (>1.87; Borrego et al., 2018), commonly interpreted as representing the presence of incompressible fluids.

Rift magmatism can have competing effects on crustal velocity. The addition of cooled mafic synrift intrusions will increase bulk crustal velocity (e.g., Korenaga et al., 2002; Keranen et al., 2004; Mackenzie et al., 2005), while a decrease in velocity would result from in situ melt, as well as warming associated with the latent heat of crystallization of melt products (e.g., Till et al., 2019). The absolute crustal velocities associated with the RVP (~3.5 and 3.6 km/s) are comparable to low-velocity anomalies associated with volcanically active segments of the Main Ethiopian Rift (range of 3–3.6 km/s; Kim et al., 2012) and the Eastern Rift in Kenya and Tanzania (~3.4–3.6; Roecker et al., 2017). For comparison, the crustal anomalies all of these rifts are much faster than those associated with inferred melt-rich bodies imaged in arcs, which are characterized by *Vs* < 3 km/s (e.g., Delph et al., 2017).

We investigated the end-member possibility of a purely thermal anomaly for the crustal velocity anomaly across a range of compositions (basalt, granite, and granulite) using the algorithms of Hacker and Abers (2004). The velocity anomaly observed at the RVP would require a temperature increase of >250°C compared to the surrounding crust (*Vs* ~ 3.7 km/s), which we consider unrealistic. We thus

interpret the reduced crustal velocity as a combination of elevated temperatures and small amounts of melt/fluids.

Within the mantle, low velocities (<4.3 km/s) extend from the Moho to at least 120-km depth beneath the RVP, with a shear velocity contrast of 5–10% slower than the rift flank to the southeast (Figure 8b). This relative velocity contrast is roughly comparable to that observed in magmatic rift segments (e.g., O'Donnell et al., 2013; Gallacher et al., 2016; Tiberi et al., 2019). However, in terms of absolute shear-wave speed, these slowest RVP velocities are fast compared to the minimum observed in magmatic segments of the Main Ethiopian Rift (<4.1 km/s; Gallacher et al., 2016), which is inferred to have a plume thermal influence and abundant partial melt (Armitage et al., 2015). Assuming the extended Burgers model of olivine anelasticity of Jackson and Faul (2010), the minimum velocities in the RVP (80- to 90-km depth) correspond to temperatures of 1200–1350°C (Figure 10). This is a reasonable range for normal asthenosphere (Faul & Jackson, 2005; Goes et al., 2012), and it is consistent with temperature estimates of olivine thermobarometry from volcanic samples from the RVP (Class et al., 2018; Mesko, 2020). At 90-km depth, it is colder than the dry solidus for a peridotitic mantle, but approaches the temperature of a “damp” solidus associated with a modest degree of hydration and/or carbonation (Dasgupta et al., 2007; Katz et al., 2003), suggesting that the melt generation is volatile induced. The composition of RVP lavas and gases is consistent with volatile-rich melting (Barry et al., 2013; De Moor et al., 2013; Furman, 1995; Hudgins et al., 2015), with relatively low rates of melt production (Barry et al., 2013; De Moor et al., 2013; Furman, 2007; Hudgins et al., 2015). The velocities are too high to permit significant retained silicate melt in the mantle; adding the additional velocity reduction associated with even small volumes ($<0.5\%$) of retained melt (Holtzman, 2016) to the solid-state calculation of Figure 10 would push the implied temperatures well below a reasonable range of damp solidi.

The relatively slow velocities between the Moho and 80-km depth (4.3 ± 0.1 km/s) with respect to the unaltered flanks suggests that the mantle lithosphere beneath the RVP has been modified by thermochemical processes (Lee et al., 2011) such that it has been effectively removed, similar to but more extensive than beneath the main rift axis. As described for the Malawi Rift axis, thermal conduction from an asthenospheric perturbation would only penetrate upward 10–20 km over a 20- to 40-Ma time scale (Turcotte & Schubert, 2014), insufficient to thermally erode the lithosphere to the degree observed. The shear velocities and thermobarometry (Class et al., 2018; Mesko, 2020) both suggest mantle temperatures that are too low for a localized thermal anomaly in the upper mantle associated with a plume source, consistent with the lack of a clear geophysical signature of a plume here in broader-scale upper mantle and transition zone imaging (Grijalva et al., 2018; Reed et al., 2016). It has been suggested that a deeper, so-called super-plume, thermal anomaly (e.g., Hansen et al., 2012) underlies much of southern Africa, and this may provide a source for the plume influence that has been detected in the youngest RVP volcanic rocks (Hilton et al., 2011). However, the seismic velocities presented here suggest that the effect of the plume on melting in this region is subtle, and that the deep mantle flux does not induce high temperatures locally in the shallow mantle. Given the relatively low temperature and the short length scale associated with the RVP anomaly, we feel that convective lithosphere removal is not a viable process for this region, and prefer a thermo-chemical modification model described in the previous section.

As in the case for weakening the rift-axis lithosphere, we hypothesize that a subtle thermal perturbation triggers low-degree partial melts that progressively permeate and weaken and/or erode the overlying lithosphere (Hopper et al., 2018). We envision that this process evolved to produce sustained volcanism of the RVP, in contrast to the apparently ephemeral and/or smaller volume production beneath the rift axis. Two scenarios can explain the greater lithospheric thinning that enabled sustained, localized magmatism at the RVP compared to the rift axis: (1) a significantly greater abundance of metasomatic material and/or (2) significantly thinner prerift lithosphere associated with prior tectonic events. The chemistry of RVP lavas show evidence for metasomatic phases like amphibole and phlogopite in their source region (Furman, 1995), and surface CO₂ venting throughout the RVP point to deep carbon venting. A greater concentration of such metasomatic phases underlying the RVP compared with the rest of the region would produce more initial melt, thus resulting in more effective erosion of the lithospheric mantle. This could in turn enable decompression melting of a damp asthenospheric source that could be sustained for ~20 Myr, which is suggested by the geochemistry of Rungwe lavas (Mesko, 2020). In this scenario, the resulting melt volumes would be sufficient to produce the observed surface volcanism.

Thinner initial lithosphere beneath the RVP would have a similar impact, in that less thermal energy associated with the metasomatic melts would be required to thermochemically modify and thin the lithosphere enough to enable sustained decompression melting of the asthenosphere. The RVP sits between the >150-km-thick TZC (e.g., Fishwick, 2010) to the north and the >200-km-thick Archean Bangweulu craton to the west (O'Donnell et al., 2013; Sarafian et al., 2018). The RVP formed above the intersection of the NE-trending Usangu and NW-SE trending Rukwa rift zones that initiated in Karoo (Permo-Triassic) time, with renewed rifting in Cretaceous, Paleogene, and Miocene-Recent time (e.g., Delvaux, 2001; Roberts et al., 2012). Although crustal stretching was relatively minor in all of these episodes, the mantle isotherms may have been elevated relative to surrounding lithosphere during sequential stretching episodes. These variations can produce lateral thermal gradients that may induce convective instabilities (Currie & van Wijk, 2015; King & Ritsema, 2000), deflect flow associated with a rising plume head (e.g., Koptev et al., 2018), and, more generally, result in zones of thinner lithosphere where warm mantle upwells (Ebinger & Sleep, 1998), inducing flux and/or decompression melting that persists through the ~20-Ma history of the RVP. Shear-wave splitting studies suggest a deflection of large-scale mantle flow around the southern edge of the TZC, and the eastern side of the Bangweulu craton (Bagley & Nyblade, 2013; Tepp et al., 2018). This general pattern is interrupted by a complex pattern of null and/or highly variable, small-magnitude splitting beneath the RVP (Tepp et al., 2018; Figure 9) that suggests a localized zone of heterogeneous mantle deformation (e.g., Courtier et al., 2010) possibly associated with thinner lithosphere in this region. The end result of either of the scenarios described above is the same: The lithosphere beneath Rungwe is thinned enough to enable sustained decompression melting of a damp asthenosphere. The geochemistry of Rungwe lavas indicates contributions from both of these asthenospheric and lithospheric components (Mesko, 2020).

The combination of preexisting relatively thin lithosphere and flux melting of lithospheric materials during the early stages of rifting to further thin the lithosphere provides the mechanism for explaining the presence of surface volcanism in the RVP, and its absence along the major rift basins. For a given concentration of fusible components and initial thermal perturbation, we infer small-degree melting along the entire rift axis, which we interpret to have facilitated weakening and lithospheric thinning. Beneath the rift basins, initial lithosphere was relatively thick, and small volumes of magmatic products stalled within the crust or shallow mantle. Beneath the RVP, initially thinner lithosphere facilitated the generation of volatile-rich melts and associated volumetrically small asthenospheric melts sufficient to penetrate to the surface (e.g., Havlin et al., 2013). The heat transfer by intrusion and crystallization and the weakening by metasomatic reactions led to strain localization that effectively weakens the entire lithospheric column (Holtzman & Kendall, 2010), enabling continued, low-level decompression melting in a damp mantle at modest temperatures.

6. Conclusions

Shear velocity imaging of the crust and upper mantle from teleseismic and ambient noise Rayleigh waves provides new constraints on the processes controlling continental extension in the weakly extended Malawi Rift. The shear velocity model is characterized by flanks of high-velocity ($>4.6 \pm 0.1$ km/s), unmodified lithosphere surrounding a zone of lower-velocity modified lithosphere beneath the RVP and the North and Central Basins of the rift. Velocities within the asthenosphere (~4.2–4.4 km/s) can be explained by normal ambient temperatures, with no clear evidence of a mantle-plume influence. Low velocities observed along the rift axis and beneath the footwall escarpments of both the North and Central Basins are attributed to thinning and thermochemical modification of the mantle lithosphere associated with ongoing extension, most likely due to flux melting-induced weakening along an ancient lithospheric suture. The prominent low-velocity anomaly within the crust and upper mantle beneath the RVP suggests modestly elevated mantle temperatures associated with volcanism, with the possibility of melt and fluids within the crust, but little to no melt in situ in the mantle. We hypothesize that the enhanced volcanic productivity within the RVP relative to the rest of the rift results from anomalously thin, fusible initial lithosphere in the RVP at the start of Cenozoic extension. Mantle velocity structure across the main rift basins is asymmetric, with the lowest lithospheric and/or asthenospheric velocities centered beneath the rift axis and border faults suggesting a coupling between localized weakening (faulting) in the crust and zones of weakening in the underlying mantle during early stage rifting.

Acknowledgments

The authors gratefully acknowledge all of those involved in acquiring the data used in this study. Seismic data used in this study are available through the Incorporated Research Institutions for Seismology (IRIS) Data Management Center (<http://ds.iris.edu/ds/nodes/dmc/>) network code YQ. This research was supported by National Science Foundation (NSF) Grants EAR-1110921, 1109293, 1109302, and 1110882, by Lamont-Doherty Earth Observatory of Columbia University, and by an NSF Graduate Research Fellowship to Accardo.

References

- Accardo, N. J. (2018). Constraints on the structure and evolution of the Malawi Rift from active- and passive-source seismic imaging (Ph.D. thesis). Columbia University, New York, USA.
- Accardo, N. J., Gaherty, J. B., Shillington, D. J., Ebinger, C. J., Nyblade, A. A., Mbogoni, G., et al. (2017). Surface-wave imaging of the weakly-extended Malawi Rift from ambient-noise and teleseismic Rayleigh waves from onshore and lake-bottom seismometers. *Geophys. J. Int.*, 209, 1892–1905.
- Accardo, N. J., Shillington, D. J., Gaherty, J. B., Scholz, C. A., Nyblade, A. A., Chindandali, P. R. N., et al. (2018). Constraints on rift basin structure and border fault growth in the Northern Malawi Rift 1 from 3-D seismic refraction imaging. *Journal of Geophysical Research: Solid Earth*, 123, 10,003–10,025. <https://doi.org/10.1029/2018JB016504>
- Adams, A., Miller, J., & Accardo, N. (2018). Relationships between lithospheric structures and rifting in the East African rift system: A Rayleigh wave tomography study. *Geochemistry, Geophysics, Geosystems*, 19(10), 3793–3810. <http://doi.org/10.1029/2018GC007750>
- Armitage, J. J., Ferguson, D. J., Goes, S., Hammond, J. O. S., Calais, E., Rychert, C. A., & Harmon, N. (2015). Upper mantle temperature and the onset of extension and break-up in Afar, Africa. *Earth and Planetary Science Letters*, 418(C), 78–90.
- Bagley, B., & Nyblade, A. A. (2013). Seismic anisotropy in eastern Africa, mantle flow, and the African superplume. *Geophysical Research Letters*, 40, 1500–1505. <https://doi.org/10.1002/grl.50315>
- Barry, P. H., Hilton, D. R., Fischer, T. P., De Moor, J. M., Mangasini, F., & Ramirez, C. (2013). Helium and carbon isotope systematics of cold “mazuku” CO₂ vents and hydrothermal gases and fluids from Rungwe Volcanic Province, southern Tanzania. *Chemical Geology*, 339, 141–156.
- Boniface, N., & Schenk, V. (2012). Neoproterozoic eclogites in the Paleoproterozoic Ubendian Belt of Tanzania: Evidence for a Pan-African suture between the Bangweulu Block and the Tanzania Craton. *Precambrian Research*, 208–211, 72–89.
- Borrego, D. J., Nyblade, A. A., Accardo, N., Gaherty, J. B., Ebinger, C. J., Shillington, D. J., et al. (2018). Crustal structure surrounding the northern Malawi Rift and beneath the Rungwe Volcanic Province, East Africa. *Geophysical Journal International*, 215, 14,140–14,260.
- Bott, M. H. P. (1991). Ridge push and associated plate interior stress in normal and hot spot regions. *Tectonophysics*, 200, 17–32. [http://doi.org/10.1016/0040-1951\(91\)90003-B](http://doi.org/10.1016/0040-1951(91)90003-B)
- Branchu, P., Bergonzini, L., Delvaux, D., De Batist, M., Golubev, V., Benedetti, M., & Klerkx, J. (2005). Tectonic, climatic and hydrothermal control on sedimentation and water chemistry of northern Lake Malawi (Nyasa), Tanzania. *Journal of African Earth Sciences*, 43, 433–446. <http://doi.org/10.1016/j.jafrearsci.2005.09.004>
- Brune, S., Heine, C., Perez-Gussinye, M., & Sobolev, S. V. (2014). Rift migration explains continental margin asymmetry and crustal hyper-extension. *Nature Communications*, 5, 4014.
- Buck, W. R. (2006). The role of magma in the development of the Afro-Arabian Rift System. *Geological Society, London, Special Publications*, 259(1), 43–54. <https://doi.org/10.1144/gsl.sp.2006.259.01.05>
- Class, C., Mesko, G.T., Plank, T.A., Boniface, N., & Manya, S. (2018). Thermobarometry of silica-undersaturated rocks on the example of the Rungwe volcanic Province, Tanzania, East Africa, Abstract V53-B08, American Geophysical Union 2018 Fall Meeting, Washington, DC.
- Corti, G., Bonini, M., Conticelli, S., Innocenti, F., Manetti, P., & Sokoutis, D. (2003). Analogue modelling of continental extension: A review focused on the relations between the patterns of deformation and the presence of magma. *Earth-Science Reviews*, 63(3–4), 169–247. [http://doi.org/10.1016/S0012-8252\(03\)00035-7](http://doi.org/10.1016/S0012-8252(03)00035-7)
- Corti, G., Calignano, E., Petit, C., & Sani, F. (2011). Controls of lithospheric structure and plate kinematics on rift architecture and evolution: An experimental modeling of the Baikal rift. *Tectonics*, 30, TC3011. <http://doi.org/10.1029/2011TC002871>
- Courtier, A. M., Gaherty, J. B., Revenaugh, J., Bostock, M. G., & Garnero, E. J. (2010). Seismic anisotropy associated with continental lithosphere accretion beneath the CANOE array, northwestern Canada. *Geology*, 38, 887–890. <https://doi.org/10.1130/G31120.1>
- Craig, T. J., Jackson, J. A., Priestley, K., & McKenzie, D. (2011). Earthquake distribution patterns in Africa: Their relationship to variations in lithospheric and geological structure, and their rheological implications. *Geophysical Journal International*, 185(1), 403–434. <http://doi.org/10.1111/j.1365-246X.2011.04950.x>
- Currie, C. A., & van Wijk, J. (2015). How craton margins are preserved insights from geodynamic models. *Journal of Geodynamics*, 100, 144–158.
- Dasgupta, R., Hirschmann, M. M., & Smith, N. D. (2007). Partial melting experiments of peridotite + CO₂ at 3 GPa and genesis of alkali ocean island basalts. *Journal of Petrology*, 48, 2093–2024.
- De Moor, J. M., Fischer, T. P., Sharp, Z. D., Hilton, D. R., Barry, P. H., Mangasini, F., & Ramirez, C. (2013). Gas chemistry and nitrogen isotope compositions of cold mantle gases from Rungwe Volcanic Province, southern Tanzania. *Chemical Geology*, 339, 30–42.
- Delph, J. R., Ward, K. M., Zandt, G., Dueca, M. N., & Beck, S. L. (2017). Imaging a magma plumbing system from MASH zone to magma reservoir. *Earth and Planetary Science Letters*, 457, 313–324. <http://doi.org/10.1016/j.epsl.2016.10.008>
- Delvaux, D. (2001). Karoo rifting in western Tanzania: Precursor of Gondwana break-up? In R. H. Weiss (Ed.), *Contributions to geology and palaeontology of Gondwana in honour of Helmut Wopfner*, (pp. 111–125). Cologne: University of Cologne.
- Ebinger, C. (2005). Continental break-up: The East African perspective. *Astronomy & Geophysics*, 46, 2.16–12.21. <https://doi.org/10.1111/j.1468-4004.2005.46216.x>
- Roecker, S., Ebinger, C., Tiberi, C., Mulibio, G., Ferdinand-Wambura, R., Mtetala, K., et al. (2017). Subsurface images of the eastern rift, Africa, from the joint inversion of body waves, surface waves and gravity: Investigating the role of fluids in early-stage continental rifting. *Geophysical Journal International*, 210, 931–950.
- Ebinger, C. J., Deino, A. L., Drake, E., & Tessa, A. L. (1989). Chronology of volcanism and rift basin propagation: Rungwe Volcanic Province, East Africa. *Journal of Geophysical Research*, 94, 15,785–15,803.
- Ebinger, C. J., Karner, G. D., & Weissel, J. K. (1991). Mechanical strength of extended continental lithosphere: Constraints from the Western Rift System, East Africa. *Tectonics*, 10(6), 1239–1256.
- Ebinger, C. J., Keir, D., Bastow, I. D., Whaler, K., Hammond, J. O. S., Ayele, A. A., et al. (2017). Crustal structure of active deformation zones in Africa: Implications for global crustal processes. *Tectonics*, 36, 3298–3332. <https://doi.org/10.1002/2017TC004526>
- Ebinger, C. J., Oliva, S. J., Pham, T.-Q., Peterson, K., Chindandali, P. R. N., Illsley-Kemp, F., et al. (2019). Kinematics of active deformation in the Malawi Rift, Africa. *Geochemistry, Geophysics, Geosystems*, 20, 3928–3951. <https://doi.org/10.1029/2019GC008354>
- Ebinger, C. J., Rosendahl, B. R., & Reynolds, D. J. (1987). Tectonic model of the Malawi Rift, Africa. *Tectonophysics*, 141(1–3), 215–235. [http://doi.org/10.1016/0040-1951\(87\)90187-9](http://doi.org/10.1016/0040-1951(87)90187-9)
- Ebinger, C. J., & Scholz, C. A. (2012). Continental rift basins: The East Africa perspective. In C. Busby, & A. Azor (Eds.), *Tectonics of sedimentary basins recent advances*, (1st ed., pp. 185–208). <https://doi.org/10.1002/9781444347166.ch9>

- Ebinger, C. J., & Sleep, N. H. (1998). Cenozoic magmatism throughout East Africa resulting from impact of a single plume. *Nature*, 395, 788–791.
- Faul, U., & Jackson, I. (2005). The seismological signature of temperature and grain size variations in the upper mantle. *Earth and Planetary Science Letters*, 234, 119–134. <http://doi.org/10.1016/j.epsl.2005.02.008>
- Fishwick, S. (2010). Surface wave tomography: Imaging of the lithosphere–asthenosphere boundary beneath central and southern Africa? *Lithos*, 120, 63–73.
- Foley, S. F., & Fischer, T. P. (2017). An essential role for continental rifts and lithosphere in the deep carbon cycle. *Nature Geoscience*, 10, 897–902.
- Fontijn, K., Ernst, G. G. J., Elburg, M. A., Williamson, D., Abdallah, E., Kwelwa, S., et al. (2010). Holocene explosive eruptions in the Rungwe Volcanic Province, Tanzania. *Journal of Volcanology and Geothermal Research*, 196(1–2), 91–110.
- Fontijn, K., Williamson, D., Mbede, E., & Ernst, G. G. J. (2012). The Rungwe Volcanic Province, Tanzania—A volcanological review. *Journal of African Earth Sciences*, 63(C), 12–31. <http://doi.org/10.1016/j.jafrearsci.2011.11.005>
- French, S. W., & Romanowicz, B. (2015). Broad plumes rooted at the base of Earth's mantle beneath major hotspots. *Nature*, 525(7567), 95–99. <https://doi.org/10.1038/nature14876>
- Fritz, H., Abdelsalam, M., Ali, K. A., Bingen, B., Collins, A. S., Fowler, A. R., et al. (2013). Orogen styles in the East African Orogen: A review of the Neoproterozoic to Cambrian tectonic evolution. *Journal of the African Earth Sciences*, 86, p. 65–106.
- Furman, T. (1995). Melting of metasomatized subcontinental lithosphere: Undersaturated mafic lavas from Rungwe, Tanzania. *Contributions to Mineral Petrology*, 122, 97–115.
- Furman, T. (2007). Geochemistry of East African Rift basalts: An overview. *Journal of African Earth Sciences*, 48(2–3), 147–160. <http://doi.org/10.1016/j.jafrearsci.2006.06.009>
- Furman, T., & Graham, D. (1999). Erosion of the lithospheric mantle beneath the East African Rift system: Geochemical evidence from the Kivu volcanic province. *Lithos*, 48, 237–262.
- Furman, T., Nelson, W. R., & Elkins-Tanton, L. T. (2016). Evolution of the East African rift: Drip magmatism, lithospheric thinning and mafic volcanism. *Geochimica et Cosmochimica Acta*, 185, 418–434.
- Gaherty, J. B., & Dunn, R. A. (2007). Evaluating hotspot-ridge interaction in the Atlantic from regional-scale seismic observations. *Geochemistry, Geophysics, Geosystems*, 8, Q05006. <https://doi.org/10.1029/2006GC001533>
- Gallacher, R. J., Keir, D., Harmon, N., Stuart, G., Leroy, S., Hammond, J. O. S., et al. (2016). The initiation of segmented buoyancy-driven melting during continental breakup. *Nature Communications*, 7, ncomms13110. <http://doi.org/10.1038/ncomms13110>
- Goes, S., Armitage, J. J., Harmon, N., Smith, H., & Huismans, R. (2012). Low seismic velocities below mid-ocean ridges: Attenuation versus melt retention. *Journal of Geophysical Research*, 117, B12403. <https://doi.org/10.1029/2012JB009637>
- Grijalva, A., Nyblade, A. A., Homann, K., Accardo, N. J., Gaherty, J. B., Ebinger, C. J., et al. (2018). Seismic evidence for plume- and craton-influenced upper mantle structure beneath northern Malawi Rift and the Rungwe volcanic province, East Africa. *G-cubed*, 19(10), 3980–3994. <https://doi.org/10.1029/2018GC007730>
- Hacker, B. R., & Abers, G. A. (2004). Subduction Factory 3: An Excel worksheet and macro for calculating the densities, seismic wave speeds, and H₂O contents of minerals and rocks at pressure and temperature. *Geochemistry, Geophysics, Geosystems*, 5, Q01005. <http://doi.org/10.1029/2003GC000614>
- Hansen, S. E., Nyblade, A. A., & Benoit, M. H. (2012). Mantle structure beneath Africa and Arabia from adaptively parameterized P-wave tomography: Implications for the origin of Cenozoic Afro-Arabian tectonism. *Earth and Planetary Science Letters*, 319–320(C), 23–34. <http://doi.org/10.1016/j.epsl.2011.12.023>
- Havlin, C., Parmentier, E. M., & Hirth, G. (2013). Dike propagation driven by melt accumulation at the lithosphere–asthenosphere boundary. *Earth and Planetary Science Letters*, 376, 20–28.
- Herrmann, R. B. (2013). Computer programs in seismology: An evolving tool for instruction and research. *Seismological Research Letters*, 84(6), 1081–1088.
- Hilbert-Wolf, H., Roberts, E., Downie, B., Mtelela, C., Stevens, N., & O'Connor, P. (2017). Application of U-Pb detrital zircon geochronology to drill cuttings for age control in hydrocarbon exploration wells: a case example from the Rukwa Rift Basin, Tanzania. *AAPG Bulletin*, 101, 143–159.
- Hilton, D. R., Halldórsson, S. A., Barry, P. H., Fischer, T. P., de Moor, J. M., Ramirez, C. J., et al. (2011). Helium isotopes at Rungwe Volcanic Province, Tanzania, and the origin of East African Plateaux. *Geophysical Research Letters*, 38, L21304. <https://doi.org/10.1029/2011GL049589>
- Hodgson, I., Illsley-Kemp, F., Gallacher, R. J., Keir, D., Ebinger, C. J., & Mtelela, K. (2017). Crustal structure at a young continental rift: A receiver function study from the Tanganyika Rift. *Tectonics*, 36, 2806–2822. <https://doi.org/10.1002/2017TC004477>
- Holtzman, B. K. (2016). Questions on the existence, persistence, and mechanical effects of a very small melt fraction in the asthenosphere. *Geochemistry, Geophysics, Geosystems*, 17, 470–484. <http://doi.org/10.1002/2015GC006102>
- Holtzman, B. K., & Kendall, J.-M. (2010). Organized melt, seismic anisotropy, and plate boundary lubrication. *Geochemistry, Geophysics, Geosystems*, 11, Q0AB06. <https://doi.org/10.1029/2010GC003296>
- Hopper, E., Gaherty, J. B., Shillington, D. J., Accardo, N. J., Nyblade, A. A., Ebinger, C. J., et al. (2018). Enhanced lithospheric mantle thinning in the melt-poor Malawi Rift. *Eos, Transactions Fall Meeting*, Washington, D.C., 10–14 Dec.
- Hopper, J. R., Dahl-Jensen, T., Holbrook, W. S., Larsen, H. C., Lizarralde, D., Korenaga, J., et al. (2003). Structure of the SE Greendland margin from seismic reflection and refraction data: Implications for nascent spreading center subsidence and asymmetric crustal accretion during North Atlantic opening. *Journal of Geophysical Research*, 108(B5), 2269. <https://doi.org/10.1029/2002JB001996>
- Hudgins, T. R., Mukasa, S. B., Simon, A. C., Moore, G., & Barifaijo, E. (2015). Melt inclusion evidence for CO₂-rich melts beneath the western branch of the East African Rift: Implications for long-term storage of volatiles in the deep lithospheric mantle. *Contributions to Mineralogy and Petrology*, 169(5), 1–18. <https://doi.org/10.1007/s00410-015-1140-9>
- Jackson, I., & Faul, U. H. (2010). Grainsize-sensitive viscoelastic relaxation in olivine: Towards a robust laboratory-based model for seismological application. *Physics of the Earth and Planetary Interiors*, 183(1–2), 151–163. <http://doi.org/10.1016/j.pepi.2010.09.005>
- Jakovlev, A., Rümpker, G., Schmeling, H., Koulakov, I., Lindenfeld, M., & Wallner, H. (2013). Seismic images of magmatic rifting beneath the western branch of the East African rift. *Geochemistry, Geophysics, Geosystems*, 14, 4906–4920. <https://doi.org/10.1002/2013GC004939>
- Jin, G., & Gaherty, J. B. (2015). Surface wave phase-velocity tomography based on multichannel cross-correlation. *Geophysical Journal International*, 201(3), 1383–1398. <http://doi.org/10.1093/gji/gjv079>
- Jin, G., Gaherty, J. B., Abers, G. A., Kim, Y., Eilon, Z., & Buck, W. R. (2015). Crust and upper mantle structure associated with extension in the Woodlark Rift, Papua New Guinea from Rayleigh-wave tomography. *Geochemistry, Geophysics, Geosystems*, 16, 3808–3824. <https://doi.org/10.1002/2015GC005840>

- Katz, R. F., Spiegelman, M., & Langmuir, C. H. (2003). A new parameterization of hydrous mantle melting. *Geochemistry, Geophysics, Geosystems*, 4(9), 1073. <https://doi.org/10.1029/2002GC000433>
- Keranen, K., Klemperer, S. L., Gloaguen, R., & EAGLE Working Group (2004). Three-dimensional seismic imaging of a protoridge axis in the Main Ethiopian rift. *Geology*, 32(11), 949.
- Kim, S., Nyblade, A. A., Rhie, J., Baag, C.-E., & Kang, T.-S. (2012). Crustal Swave velocity structure of the Main Ethiopian Rift from ambient noise tomography. *Geophysical Journal International*, 191, 865–878. <https://doi.org/10.1111/j.1365-246X.2012.05664.x>
- King, R., Floyd, M., Reilinger, R., & Bendick, R. (2019). GPS velocity field (MIT 2019.0) for the East African Rift System generated by King et al., 10.1594/IEDA/324785 ed, interdisciplinary earth data alliance (IEDA). <https://doi.org/10.1594/IEDA/324785>
- King, S. D., & Anderson, D. L. (1995). An alternative mechanism of flood basalt formation. *Earth and Planetary Science Letters*, 136, 269–279.
- King, S. D., & Ritsema, J. (2000). African hot spot volcanism: Small-scale convection in the upper mantle beneath Cratons. *Science*, 290(5494), 1137–1140. <https://doi.org/10.1126/science.290.5494.1137>
- Koptev, A., Cloetingh, S., Gerya, T., Calais, E., & Leroy, S. (2018). Non-uniform splitting of a single mantle plume by double cratonic roots: Insight into the origin of the central and southern East African Rift System. *Terra Nova*, 30(2), 125–134.
- Korenaga, J., Kelemen, P. B., & Holbrook, W. S. (2002). Methods for resolving the origin of large igneous provinces from crustal seismology. *Journal of Geophysical Research*, 107(B9), 2178. <https://doi.org/10.1029/2001JB001030>
- Lavayssi  re, A., Drooff, C., Ebinger, C., Gallacher, R., Illsley-Kemp, F., Oliva, S. J., & Keir, D. (2019). Depth extent and kinematics of faulting in the southern Tanganyika rift, Africa. *Tectonics*, 38, 842–862. <https://doi.org/10.1029/2018TC005379>
- Lee, C.-T. A., Luffi, P., & Chin, E. J. (2011). Building and destroying continental mantle. *Annual Review of Earth and Planetary Sciences*, 39(1), 59–90. <http://doi.org/10.1146/annurev-earth-040610-133505>
- Lin, F.-C., & Ritzwoller, M. H. (2011). Helmholtz surface wave tomography for isotropic and azimuthally anisotropic structure. *Geophysical Journal International*, 186, 1104–1120. <https://doi.org/10.1111/j.1365-246X.2011.05070.x>
- Lizarralde, D., Gaherty, J. B., Collins, J. A., Hirth, G., & Kim, S. (2004). Spreading-rate dependence of melt extraction at mid-ocean ridges from far-offset seismic data. *Nature*, 432(7018), 744–747. <https://doi.org/10.1038/nature03140>
- Lyons, R. P., Scholz, C. A., Buonocore, M. R., & Martin, M. R. (2011). Late Quaternary stratigraphic analysis of the Lake Malawi Rift, East Africa: An integration of drill-core and seismic-reflection data. *Palaeogeography, Palaeoclimatology, Palaeoecology*, 303(1–4), 20–37. <http://doi.org/10.1016/j.palaeo.2009.04.014>
- Mackenzie, G. D., Thybo, H., & Maguire, P. K. H. (2005). Crustal velocity structure across the Main Ethiopian Rift: Results from two-dimensional wide-angle seismic modeling. *Geophysical Journal International*, 162, 994–1006.
- Menke, W., & Jin, G. (2015). Waveform fitting of cross spectra to determine phase velocity using Aki's formula. *Bulletin of the Seismological Society of America*, 105(3), 1619–1627. <http://doi.org/10.1785/0120140245>
- Mesko, G. T. (2020). *Magmatism at the southern end of the East African Rift System: Origin and role during early stage melting* (pp. 516). New York: Columbia University.
- Muirhead, J. D., Kattenhorn, S. A., Lee, H., Mana, S., Turrin, B. D., Fischer, T. P., et al. (2016). Evolution of upper crustal faulting assisted by magmatic volatile release during early-stage continental rift development in the East African Rift. *Geosphere*, 12(6), 1670–1700.
- Mulibo, G. D., & Nyblade, A. A. (2016). The seismotectonics of Southeastern Tanzania: Implications for the propagation of the eastern branch of the East African Rift. *Tectonophysics*, 674, 20–30. <http://doi.org/10.1016/j.tecto.2016.02.009>
- Nettles, M., & Dziewonski, A. M. (2008). Radially anisotropic shear velocity structure of the upper mantle globally and beneath North America. *Journal of Geophysical Research*, 113, B02303. <https://doi.org/10.1029/2006JB004819>
- Nixon, C. W., McNeill, L. C., Bull, J. M., Bell, R. E., Gawthorpe, R. L., Henstock, T. J., et al. (2016). Rapid spatiotemporal variations in rift structure during development of the Corinth Rift, Central Greece. *Tectonics*, 35, 1225–1248. <https://doi.org/10.1002/2015TC004026>
- Nyblade, A. (2007). AfricaArray. International Federation of Digital Seismograph Networks. Dataset/Seismic Network. https://doi.org/10.7914/SN/ZP_2007
- Nyblade, A. A., & Pollack, H. N. (1993). A global analysis of heat flow in Precambrian terrains: Implications for the thermal structure of Archean and Proterozoic lithosphere. *Journal of Geophysical Research*, 92, 12,207–12,218. <http://doi.org/10.1029/93JB00521>
- O'Donnell, J. P., Adams, A., Nyblade, A. A., Mulibo, G. D., & Tugume, F. (2013). The uppermost mantle shear wave velocity structure of eastern Africa from Rayleigh wave tomography: Constraints on rift evolution. *Geophysical Journal International*, 194(2), 961–978. <http://doi.org/10.1093/gji/ggt135>
- O'Donnell, J. P., Selway, K., Nyblade, A. A., Brazier, R. A., Tahir, N. E., & Durrheim, R. J. (2016). Thick lithosphere, deep crustal earthquakes and no melt: A triple challenge to understanding extension in the western branch of the East African Rift. *Geophysical Journal International*, 204(2), 985–998. <http://doi.org/10.1093/gji/ggv492>
- Priestley, K., & McKenzie, D. (2006). The thermal structure of the lithosphere from shear wave velocities. *Earth and Planetary Science Letters*, 24, 285–301.
- Rau, C. J., & Forsyth, D. W. (2011). Melt in the mantle beneath the amagmatic zone, southern Nevada. *Geology*, 39(10), 975–978. <http://doi.org/10.1130/G32179.1>
- Reed, C. A., Liu, K. H., Chindandali, P. R. N., Massingue, B., Mdala, H., Mutamina, D., et al. (2016). Passive rifting of thick lithosphere in the southern East African Rift: Evidence from mantle transition zone discontinuity topography. *Journal of Geophysical Research: Solid Earth*, 121, 8068–8079. <http://doi.org/10.1002/2016JB013131>
- Regenauer-Lieb, K., Rosenbaum, G., & Weinberg, R. F. (2008). Strain localisation and weakening of the lithosphere during extension. *Tectonophysics*, 458(1–4), 96–104. <http://doi.org/10.1016/j.tecto.2008.02.014>
- Roberts, E. M., Stevens, N. J., & O'Connor, P. M. (2012). Initiation of the western branch of the east African Rift coeval with the eastern branch. *Nature Geoscience*, 5(4), 289–294. <http://doi.org/10.1038/ngeo1432>
- Sarafian, E., Evans, R. L., Abdelsalam, M. G., Atekwana, E., Elsenbeck, J., Jones, A. G., & Chikambwe, E. (2018). Imaging Precambrian lithospheric structure in Zambia using electromagnetic methods. *Gondwana Research*, 54, 38–49. <http://doi.org/10.1016/j.gr.2017.09.007>
- Scholz, C. A., Rosendahl, B. R., Versfelt, J. W., Kaczmarick, K. J., Schwede, W., & Woods, L. D. (1989). Seismic Atlas of Lake Malawi (Nyasa), East Africa. Duke University, Durham, NC: Project PROBE, Geology Dept.
- Scholz, C. A., Shillington, D. J., Wright, L. J. M., Accardo, N., Gaherty, J. B., & Chindandali, P. (2020). Intrarift fault fabric, segmentation, and basin evolution of the Lake Malawi (Nyasa) Rift, East Africa. *Geosphere*, 16, 2020. <https://doi.org/10.1130/GES02228.1>
- Shillington, D. J., Gaherty, J. B., Ebinger, C. J., Scholz, C. A., Selway, K., Nyblade, A. A., et al. (2016). Acquisition of a unique onshore/offshore geophysical and geochemical dataset in the northern Malawi (Nyasa) rift. *Seismological Research Letters*, 87. <https://doi.org/10.1785/0220160112>

- Shillington, D. J., Holbrook, W. S., Van Avendonk, H. J. A., Tucholke, B. E., Hopper, J. R., Louden, K. E., et al. (2006). Evidence for asymmetric nonvolcanic rifting and slow incipient oceanic accretion from seismic reflection data on the Newfoundland margin. *Journal of Geophysical Research*, 111, B09402. <https://doi.org/10.1029/2005JB003981>
- Shillington, D. J., Scholz, C. A., Chindandali, P. R. N., Gaherty, J. B., Accardo, N. J., Onyango, E., et al. (2020). Controls on intrarift faulting in the North Basin of the Malawi (Nyasa) Rift, East Africa. *Tectonics*, 39, e2019TC005633. <https://doi.org/10.1029/2019TC005633>
- Stamps, D. S., Flesch, L. M., Calais, E., & Ghosh, A. (2014). Current kinematics and dynamics of Africa and the East African Rift system. *Journal of Geophysical Research: Solid Earth*, 119, 5161–5186. <https://doi.org/10.1002/2013JB010717>
- Stamps, D. S., Saria, E., & Kreemer, C. (2018). A geodetic strain rate model for the east African rift system. *Scientific Reports*, 8. <https://doi.org/10.1038/s41598-41017-19097-w>
- Tepp, G., Ebinger, C. J., Zal, H., Gallacher, R., Accardo, N., Shillington, D. J., et al. (2018). Seismic anisotropy of the upper mantle below the Western Rift, East Africa. *Journal of Geophysical Research: Solid Earth*, 123, 5644–5660. <https://doi.org/10.1029/2017JB015409>
- Thybo, H., & Nielsen, C. A. (2009). Magma-compensated crustal thinning in continental rift zones. *Nature*, 457(7231), 873–876. <https://doi.org/10.1038/nature07688>
- Tiberi, C., Gautier, S., Ebinger, C., Roecker, S., Plasman, M., Albaric, J., et al. (2019). Lithospheric modification by extension and magmatism at the craton-orogenic boundary: North Tanzania Divergence, East Africa. *Geophysical Journal International*, 216, 1693–1710.
- Till, C. B., Kent, A. J. R., Abers, G. A., Janiszewski, H. A., Gaherty, J. B., & Pitcher, B. (2019). Towards assessing the causes of volcanic diversity at the arc scale. *Nature Communications*, 10(1), 1–12. <https://doi.org/10.1038/s41467-019-09113-0>
- Turcotte, D., & Schubert, G. (2014). *Geodynamics*. Cambridge: Cambridge University Press.
- Van Avendonk, H. J. A., Holbrook, W. S., Nunes, G. T., Shillington, D. J., Tucholke, B. E., Louden, K. E., et al. (2006). Seismic velocity variations across the rifted margin of the eastern Grand Banks, Canada. *Journal of Geophysical Research*, 111, B11404. <https://doi.org/10.11029/12005JB004156>
- Weissel, J. K., & Karner, G. D. (1989). Flexural uplift of rift flanks due to mechanical unloading of the lithosphere during extension. *Journal of Geophysical Research*, 94, 13,919–13,950.
- Whitmarch, R. B., Manatschal, G., & Minshull, T. A. (2001). Evolution of magma-poor continental margins from rifting to seafloor spreading. *Nature*, 413, 150–153.
- Wölbern, I., Rümpker, G., Link, K., & Sodoudi, F. (2012). Melt infiltration of the lower lithosphere beneath the Tanzania craton and the Albertine rift inferred from S receiver functions. *Geochemistry, Geophysics, Geosystems*, 13, Q0AK08. <https://doi.org/10.1029/2012GC004167>
- Wopfner, H. (2002). Tectonic and climatic events controlling deposition in Tanzanian Karoo basins. *Journal of the African Earth Sciences*, 34(p), 167–177.
- Wright, T. J., Ebinger, C., Biggs, J., Ayele, A., Yirgu, G., Keir, D., & Stork, A. (2006). Magma-maintained rift segmentation at continental rupture in the 2005 Afar dyking episode. *Nature*, 442(7100), 291–294. <https://doi.org/10.1038/nature04978>
- Yang, Z., & Chen, W.-P. (2010). Earthquakes along the East African Rift System: A multiscale, system-wide perspective. *Journal of Geophysical Research*, 115, B12309. <https://doi.org/10.1029/2009JB006779>